Title: Tuft cell-derived acetylcholine regulates epithelial fluid secretion

Authors: Tyler E. Billipp[1], Connie Fung[2], Lily M. Webeck[1], Derek B. Sargent[1], Matthew B. Gologorsky[2,3], Margaret M. McDaniel[1], Darshan N. Kasal[1], John W. McGinty[1], Kaitlyn A. Barrow[4], Lucille M. Rich[4], Alessio Barilli[5], Mark Sabat[6†], Jason S. Debley[4,7], Richard Myers[6], Michael R. Howitt[2,3], Jakob von Moltke[1*]

Affiliations:

1 Department of Immunology, University of Washington School of Medicine, Seattle, Washington, USA.

2 Department of Pathology, Stanford University School of Medicine, Stanford, CA 94305, USA

3 Department of Microbiology and Immunology, Stanford University School of Medicine, Stanford, CA 94305, USA

4 Center for Immunity and Immunotherapies, Seattle Children's Research Institute, Seattle, Washington, USA

5 Aptuit, an Evotec Company, Verona, Italy

6 Takeda Pharmaceuticals, San Diego, California, USA

7 Department of Pediatrics, Division of Pulmonary and Sleep Medicine, Seattle Children's Hospital, University of Washington, Seattle, WA, USA

* Correspondence and lead contact: jmoltke@uw.edu

† Now at Atomwise, San Francisco, California, USA

Abstract:

Tuft cells are solitary chemosensory epithelial cells that can sense lumenal stimuli at mucosal barriers and secrete effector molecules to regulate the physiology and immune state of their surrounding tissue. In the small intestine, tuft cells detect parasitic worms (helminths) and microbe-derived succinate, and signal to immune cells to trigger a Type 2 immune response that leads to extensive epithelial remodeling spanning several days. Acetylcholine (ACh) from airway tuft cells has been shown to stimulate acute changes in breathing and mucocilliary clearance, but its function in the intestine is unknown. Here we show that tuft cell chemosensing in the intestine leads to release of ACh, but that this does not contribute to immune cell activation or associated tissue remodeling. Instead, tuft cell-derived ACh triggers immediate fluid secretion from neighboring epithelial cells into the intestinal lumen. This tuft cell-regulated fluid secretion is amplified during Type 2 inflammation, and helminth clearance is delayed in mice lacking tuft cell ACh. The coupling of the chemosensory function of tuft cells with fluid secretion creates an epithelium-intrinsic response unit that effects a physiological change within seconds of activation. This response mechanism is shared by tuft cells across tissues, and serves to regulate the epithelial secretion that is both a hallmark of Type 2 immunity and an essential component of homeostatic maintenance at mucosal barriers.

63 **Introduction:**

64 The physiologic function and immune defense of mucosal tissues require fluid
65 secretion, and epithelial cells employ multiple independent mechanisms to regulate this
66 process. For example, cyclic AMP (cAMP) induces apical chloride (Cl^-) secretion from
67 epithelial cells through cystic fibrosis transmembrane conductance regulator (CFTR).[1]
68 The resulting ionic gradient draws Na^+ and then water out of the tissue and into the
69 lumen, where it hydrates mucus and can contribute to epithelial "flushing".[2,3] Loss-of-
70 function mutations in CFTR cause cystic fibrosis, a disease characterized by viscous
71 mucus, reduced lung function, and bacterial overgrowth.[1] Epithelial Cl^-/water secretion
72 can also occur via calcium-dependent ion channels, with muscarinic acetylcholine
73 receptors (mAChR) in the basolateral membrane often inducing the necessary
74 intracellular calcium flux.[2] Acetylcholine (ACh) is a canonical neurotransmitter
75 synthesized by the enzyme choline acetyltransferase (*Chat*). Neurons innervating
76 mucosal barriers can induce ACh-dependent fluid secretion, but non-neuronal sources
77 of ACh have now been widely reported in other contexts.[3–7]

78 Among epithelial cells, tuft cells are the dominant source of ACh.[8,9] Found across
79 mucosal tissues, they are a lineage of chemosensory cells that monitor the lumenal
80 microenvironment and release effectors to regulate the mucosa. *Chat* expression is part
81 of a transcriptional signature shared by all murine tuft cells[10,11,] and ChAT protein has
82 been detected in human tuft cells in the intestine and airways.[12,13] The function of tuft
83 cell-derived ACh has also been studied in several tissues. For example, tuft cells in the
84 nasal epithelium sense bitter and bacteria-derived ligands[14] and secrete ACh, which
85 signals on neurons to induce neurogenic inflammation.[15] Tracheal tuft cells activate
86 nicotinic ACh receptors (nAChRs) to cause a brief cessation in breathing[16] and
87 mAChRs on neighboring epithelial cells to increase ciliary beat frequency[8,17] in
88 response to similar ligands. Likewise, tuft cells in the urethra use ACh to activate
89 neurons and regulate urine release.[18,19] However, the function of tuft cell-derived ACh in
90 the intestine is unknown, nor has a link between tuft cells and fluid secretion been
91 tested.

92 Small intestinal (SI) tuft cells play a critical role in the initiation of "Type 2"
93 immune responses to helminth infection and colonization by *Tritrichomonas*

94 protists[20,21,22]. Tuft cells express SUCNR1, the receptor for extracellular succinate,
95 which *Tritrichomonas sp.* and the microbiota secrete as a metabolite.[11,23,24] SUCNR1
96 signaling causes intracellular Ca^{2+} flux that opens the cation channel TRPM5. The
97 resulting Na^{+} influx depolarizes the tuft cell and likely regulates secretion of most tuft
98 cell effector molecules.[25,26] *Sucnr1*$^{-/-}$ mice fail to detect *Tritrichomonas* colonization, but
99 the immune response to helminth infection is unaffected.[11,24] Nonetheless, sensing of
100 both helminths and protists is severely attenuated in *Trpm5*$^{-/-}$ mice or *Pou2f3*$^{-/-}$ mice that
101 lack tuft cells entirely.[11,20,22]

102 Once activated by lumenal signals, tuft cells produce IL-25 and, in some cases,
103 leukotriene C4 (LTC_4) to activate resident group 2 innate lymphoid cells (ILC2s) in the
104 underlying *lamina propria* (LP).[21,27] ILC2s secrete canonical Type 2 cytokines, including
105 IL-13, that collectively recruit Type 2 immune cells and coordinate intestinal remodeling.
106 Among its many targets, IL-13 produced by ILC2s signals on undifferentiated epithelial
107 cells to bias differentiation towards mucus-producing goblet cells and tuft cells.[20,21,28,29]
108 Given the 3-5 day turnover of the intestinal epithelium, this feed-forward process, known
109 as the tuft-ILC2 circuit, results in dramatic hyperplasia of both goblet cells and tuft cells,
110 the latter of which increase 10-fold.[20,21,22]

111 The Type 2 effector functions that clear worms from the intestine,[30,31] collectively
112 referred to as “weep and sweep,” require the coordination of multiple signals. In addition
113 to increasing the number of tuft and goblet cells, IL-13 upregulates production of mucus
114 and anti-helminthic/microbial peptides in the epithelium,[32,33,34] increases fluid
115 secretion,[35] and increases expression of mAChRs on smooth muscle,[36,37,38] but actual
116 secretion (“weep”) and muscle contraction (“sweep”) generally require additional
117 signals. ACh is one molecule that can acutely activate both weep and sweep,[38] and
118 mAChRs are required for helminth clearance.[39,40] Conversely, helminths secrete ACh
119 esterases (AChE), likely in an attempt to inhibit weep and sweep responses.[41,42,43] The
120 sources of ACh in Type 2 immunity, however, are not defined.

121 By sensing lumenal signals and activating ILC2s, tuft cells serve as sentinels for
122 intestinal Type 2 immunity, but the fact that many more tuft cells are generated after the
123 agonist has been detected suggests an additional effector function for these cells. Here
124 we describe such an effector function, which is independent of ILC2s. We show that in

125 response to sensing of succinate or direct activation of TRPM5, tuft cells secrete ACh to
126 induce epithelial fluid secretion in the intestine and airways. During Type 2 tissue
127 remodeling, *Chat*+ tuft cells increase in number, enhancing the fluid secretion response.
128 Upon helminth infection, mice with *Chat*-deficient tuft cells experience delayed helminth
129 clearance despite normal tuft-ILC2 circuit activation. We conclude that tuft cell-derived
130 ACh regulates epithelial fluid secretion, and that this effector function can contribute to
131 Type 2 immune responses during helminth infection.
132
133 **Results:**
134 ***SI tuft cells express Chat in a proximal to distal gradient***
135 Neuronal *Chat* is important for intestinal function, but the role of *Chat* in intestinal
136 tuft cells has not been studied. To assess *Chat* expression by tuft cells in the SI at
137 single cell resolution, we employed *Chat-GFP* transgenic reporter mice. Immunolabeling
138 for GFP colocalized with the tuft cell marker DCLK1 in both the proximal SI (pSI; first 5-
139 10 cm) and distal SI (dSI; last 5-10 cm) (Fig. 1A). By flow cytometry, >99% of GFP+
140 epithelial cells stained for the tuft cell-specific *Il25-RFP* reporter (Fig. 1B). However, not
141 all tuft cells were GFP+ (Fig. S1A), and we observed a gradient in the frequency of
142 GFP+ tuft cells that increased from 40% of all tuft cells in the pSI to 80% in the dSI (Fig.
143 1C-D). The discovery of GFP-negative tuft cells was unexpected, as the *Chat* reporter
144 marks nearly 100% of tuft cells in other tissues.[8] To validate our findings, we crossed
145 *Chat*-Cre mice, in which Cre is expressed from the endogenous *Chat* locus, to
146 *Rosa26::STOP*$^{fl/fl}$*::CAG-tdTomato* (Ai9) mice for lineage tracing. Using CD24 and
147 Siglec-F to identify tuft cells, we again observed both reporter-positive and -negative tuft
148 cells, with an increased frequency of reporter-positive tuft cells in the distal compared to
149 the proximal SI (Fig. S1B).

150

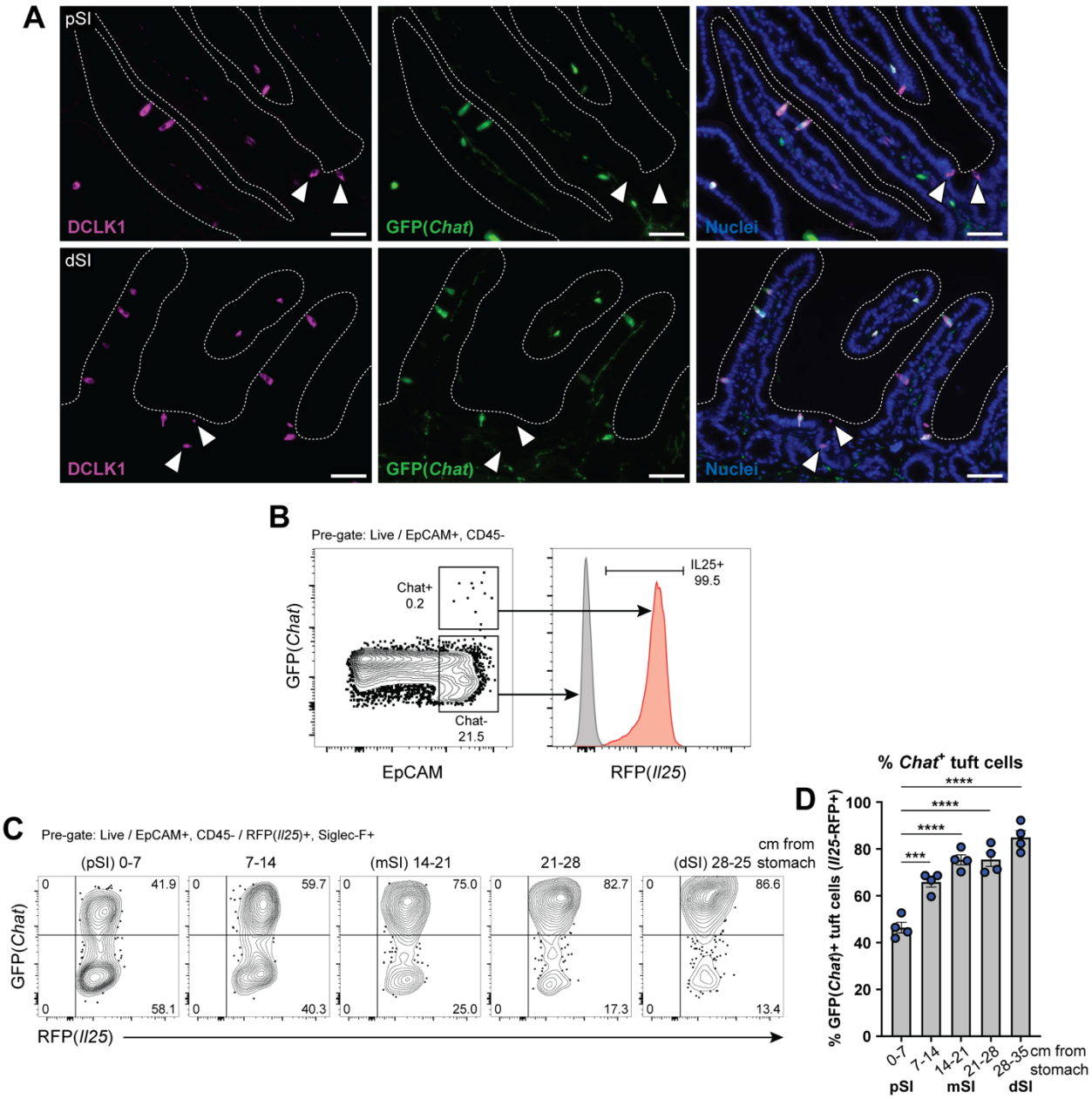

151

152 **Figure 1: SI tuft cells express *Chat* in a proximal to distal gradient.** (**A**) Representative images of
153 GFP(*Chat*) expression (green) by DCLK1+ tuft cells (magenta) in the proximal SI (pSI) and distal SI (dSI)
154 by immunofluorescence. White arrows indicate GFP(*Chat*)- tuft cells. Nuclei stained with DAPI (blue).
155 Scale bars: 50 µm (**B**) GFP+ epithelial cells (EpCAM+) are RFP(*Il25*)+ tuft cells. (**C** and **D**) (C)
156 Representative flow cytometry and (D) quantification of the percentage of GFP+ tuft cells by sequential 7
157 cm section across the length of the SI. In D, each symbol represents an individual mouse (columns
158 represent different tissues from same mouse) from three pooled experiments. *p < 0.05, **p < 0.01, ***p <

159 0.001 by one way ANOVA with Tukey's multiple comparisons test (D). mSI, medial SI. Graphs depict
160 mean +/- SEM. Also see Figure S1.
161
162 Given the binary nature of *Chat-GFP* expression in SI tuft cells, we hypothesized
163 that *Chat* might mark transcriptionally distinct tuft cell subsets. We therefore sorted
164 GFP+ and GFP- tuft cells, performed bulk RNA sequencing, and identified differentially
165 expressed genes (DEGs) (Fig. S1C, Table S1, Data File S1). Surprisingly, despite the
166 binary nature of GFP expression, *Chat* was downregulated only 2.8-fold (FDR = .0009)
167 in GFP- cells, suggesting translation is regulated via untranslated regions of the
168 endogenous *Chat* transcript that are retained in the transgene (Fig. S1C). More broadly,
169 even with a lenient fold-change (FC) cutoff of 2 (FDR <.01), there were only 105 DEGs.
170 None of the downregulated genes were part of the SI tuft cell signature,[44] but *Sucnr1*
171 (FC = 3.3, FDR = .0007) and the downstream G alpha subunit *Gnat3* (FC = 4.9, FDR =
172 .0001) were upregulated in GFP+ cells (Fig S1C, Table S1). Comparing *Chat*+ tuft cells
173 to previously reported intestinal tuft cell subsets "Tuft-1" and "Tuft-2",[9] we found greater
174 enrichment for Tuft-2 genes (Fig. S1D), but the best match was with a dSI tuft cell
175 signature we generated by sorting tuft cells from the proximal and distal 5 cm of
176 unmanipulated intestines (Fig. S1D-E, Table S2, Data File S2). This signature similarly
177 includes *Sucnr1* and *Gnat3,* and we hypothesize that transcriptional differences
178 between GFP+ and GFP- cells resulted mostly from a distal bias among sorted GFP+
179 cells, consistent with the gradient we observed (Fig. 1D).
180 We also considered the possibility that *Chat*- cells were an immature stage
181 before *Chat*+ cells, but while GFP+ cells predominated in the villi and GFP- cells in the
182 crypts, there were still GFP+ cells in the crypts and GFP- cells at the villus tips, making
183 a developmental relationship unlikely (data not shown). Both IL4ra-dependent and
184 IL4ra-independent tuft cells have been identified in the SI[45], but we found many *Chat-*
185 *GFP*+ tuft cells in the SI of *Il4ra*$^{-/-}$ mice, suggesting *Chat* expression is not exclusive to
186 IL-13-induced tuft cells (Fig. S1F). The mechanisms regulating *Chat* expression in tuft
187 cells therefore remain unknown.

Fig. S1: Related to Fig. 1

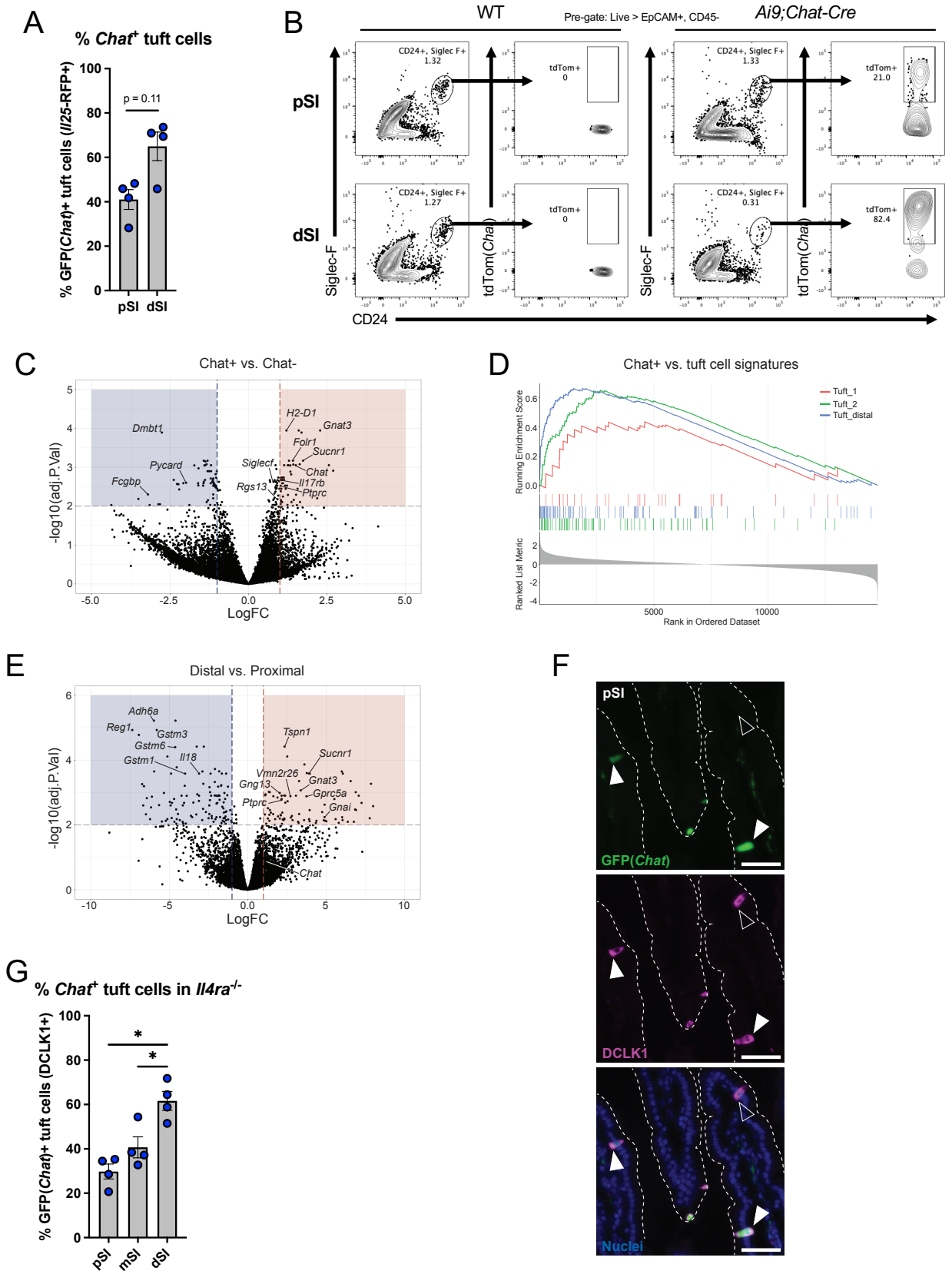

189 **Supplemental Figure 1:** (**A**) Quantification of GFP+ tuft cells (RFP+) from pSI and dSI of *Chat-*
190 *GFP*;*Il25*$^{RFP/+}$ mice by immunofluorescence (IF). (**B**) Representative flow cytometry of traced tdTom+ tuft
191 cells (CD24+, Siglec-F+) from pSI and dSI of wild-type (WT) and *Ai9;Chat-Cre* mice. (**C**) Volcano plot
192 showing log2FC of genes expressed in *Chat*+ tuft cells (n=4) versus *Chat*- tuft cells (n=3) sorted from
193 whole SI of *Chat-GFP*;*Il25*$^{RFP/+}$ mice. (**D**) Gene set enrichment analysis comparing *Chat*+ tuft cell gene
194 expression to Tuft-1 and Tuft-2 consensus gene signatures and the dSI tuft cell signature from (**E**)
195 Volcano plot showing log2FC of genes expressed in tuft cells sorted from the dSI (n=4) versus tuft cells
196 sorted from the pSI (n=4) of B6 mice. (**F**) Representative immunofluorescence image showing a GFP-
197 (green) tuft cell (DCLK1+, magenta) at the villus tip (hollow white arrow), past other GFP+ tuft cells (solid
198 white arrows). Nuclei stained with DAPI (blue). Scale bars: 50 μm. (**G**) Quantification of GFP(*Chat*)+ tuft
199 cells (DCLK1+) from denoted tissues of *Il4ra*$^{-/-}$*;Chat-GFP* mice by immunofluorescence. In the graphs,
200 each symbol represents an individual mouse (columns represent different tissues from same mouse) from
201 two pooled experiments. *$p < 0.05$, **$p < 0.01$, ***$p < 0.001$ by Mann-Whitney test (A) or one way ANOVA
202 with Tukey's multiple comparisons test (G). mSI, medial SI. Graphs depict mean +/- SEM.
203

204 ***ACh from tuft cells induces fluid secretion from the SI epithelium***

205 ACh rapidly induces fluid, mucus, and antimicrobial peptide secretion when it
206 binds muscarinic ACh receptors (mAChRs) on SI epithelial cells.[4,46,47,48] Classically,
207 enteric neurons are considered the primary source of ACh that regulates SI
208 secretion.[4,49,50] but we hypothesized that tuft cells could link lumenal chemosensing to
209 epithelial secretion via basolateral release of ACh.

210 To make sensitive, real-time measurements of SI epithelial electrophysiology, we
211 employed Ussing chambers,[51] which have been used to measure ACh-induced
212 epithelial ion flux.[52] Two chambers containing physiologic buffer are separated by a
213 piece of SI epithelium and the voltage across the epithelium is clamped. When
214 negatively charged ions (e.g. Cl^-) are secreted into the lumenal chamber, current is
215 injected into the basolateral chamber to restore the voltage (Fig. 2A). This "short-circuit"
216 current, or Isc, is directly proportional to ion flux[51].

217 To test whether tuft cells regulate ion flux, we mounted SI tissue from
218 unmanipulated mice in the Ussing chamber and stimulated with Na_2-succinate
219 (succinate), since it is the best-defined ligand for SI tuft cells.[11,23,24] When we stimulated
220 the lumenal side of the SI tissue with 10 mM succinate, we recorded a rapid increase in
221 the Isc that lasted several minutes before returning close to baseline (Fig. 2B). We

222 quantified this response by measuring the change in Isc from the baseline before
223 stimulation to its peak, known as the delta Isc (ΔIsc; see Fig. 2B inset). To control for
224 the addition of sodium, we tested NaCl at an equimolar concentration of sodium (20
225 mM). NaCl was sufficient to increase the Isc, but the response was
226 significantly smaller than the succinate response and failed to return to baseline. The
227 succinate response, on the other hand, had similar kinetics to the response elicited by
228 the ACh mimic carbachol (CCh), given basolaterally to maximally stimulate mAChRs
229 (Fig. 2B). The succinate response was greatly diminished in SI from *Sucnr1*$^{-/-}$ mice,
230 though a residual, likely sodium-dependent increase remained (Fig. S2A). To avoid the
231 sodium response, we used the synthetic SUCNR1 agonist cis-epoxysuccinic acid
232 (cESA),[53] which stimulated an Isc response comparable to succinate, but that was
233 entirely *Sucnr1*-dependent (Fig. S2A). We used cESA in place of succinate for most of
234 the subsequent Ussing experiments.
235 To further characterize the succinate/cESA Isc response, we began by testing
236 the role of epithelial polarity. cESA induced ion flux when given lumenally, but not
237 basolaterally, consistent with lumenal restriction of SUCNR1 in tuft cells (Fig. S2B).
238 Conversely, CCh stimulated ion flux when given basolaterally, but not lumenally,
239 consistent with basolateral restriction of mAChRs on intestinal epithelial cells (IECs).[4]
240 Since the Isc represents net ion flux across the epithelium, the increased Isc response
241 to succinate could be due to either increased lumenal secretion of negatively charged
242 anions (e.g. Cl^-, $HCO3^-$) or increased absorption of positively charged cations (e.g. Na^+,
243 K^+) from the lumen.[4] To test the contribution of Cl^- ions selectively, we replaced Cl^- with
244 gluconate, which cannot cross the epithelium.[51,54] and found that both the cESA and
245 CCh responses were abrogated (Fig. 2C). Bumetanide, an inhibitor of the basolateral
246 chloride transporter NKCC1 that is required for sustained Cl^- secretion,[1] likewise
247 decreased the response to cESA (Fig. S2C).

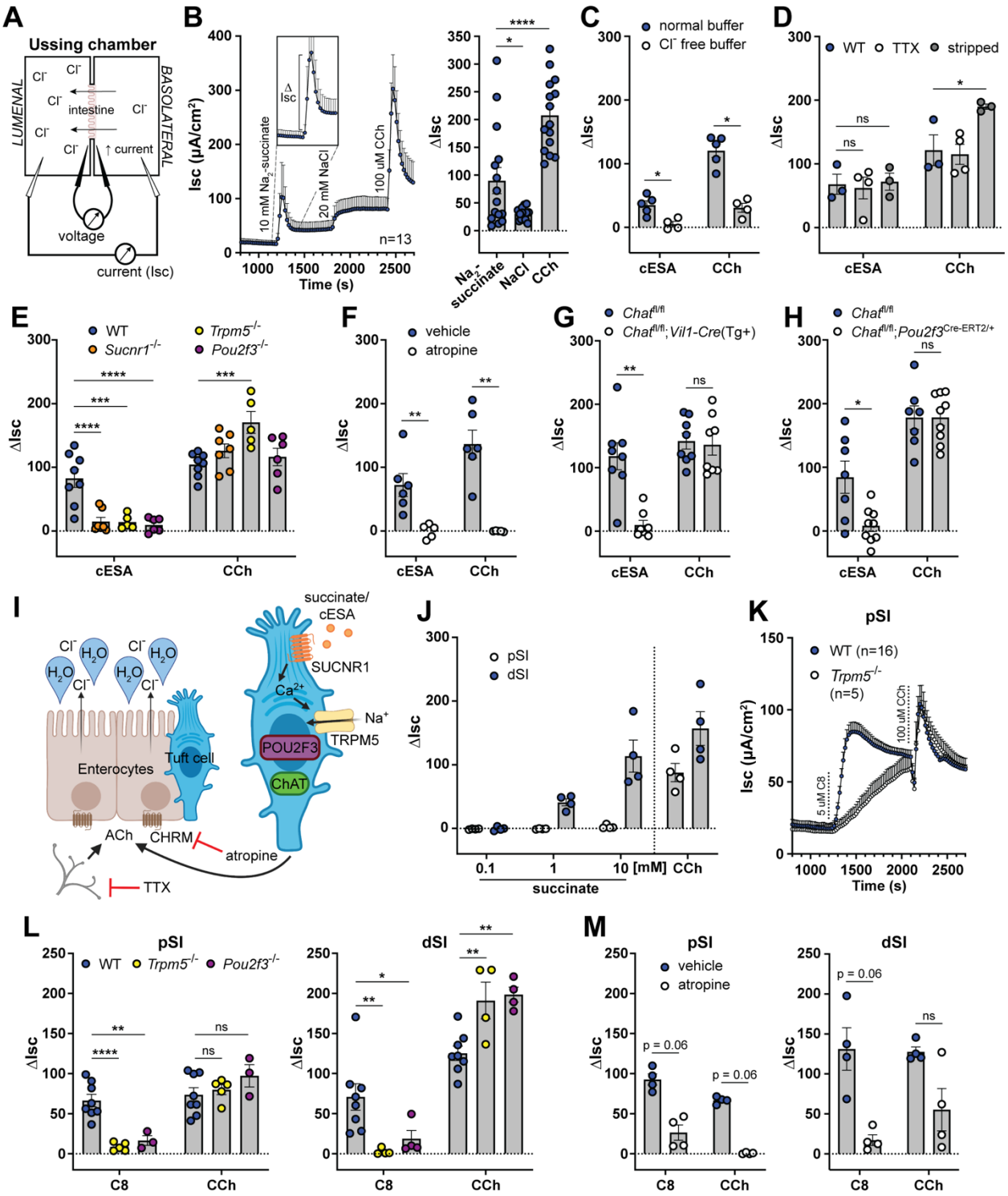

Figure 2: Tuft cell-derived ACh induces epithelial fluid secretion. (**A**) Ussing chamber schematic. (**B**) Average Isc traces and quantification of the delta Isc (ΔIsc, see inset and bar graph) of WT dSI tissue stimulated as indicated (10 mM Na_2-succinate and 20 mM NaCl, lumenal; 100 μM CCh, basolateral). (**C**)

252 ΔIsc values of WT dSI in presence of normal chloride- (Cl^-) containing buffer or buffer selectively lacking
253 Cl^-, stimulated as indicated (10 mM cESA, lumenal). (**D**) ΔIsc values of WT intact dSI compared to
254 stripped dSI and dSI pretreated 15 min with TTX (1 μM, basolateral), stimulated as indicated. (**E**) ΔIsc
255 values of dSI from mice of indicated genotypes stimulated as indicated. (**F**) ΔIsc values of WT dSI
256 compared to dSI pretreated 15 min with pan-CHRM inhibitor atropine (10 μM, basolateral), stimulated as
257 indicated. (**G** and **H**) ΔIsc values of dSI with (G) epithelial cell- (*Vil1-Cre*) and (H) tuft cell-specific
258 (*Pou2f3*$^{ERT2\text{-}Cre/+}$) *Chat* deletion, stimulated as indicated. (**I**) Model of tuft cell chemosensing of succinate
259 driving ACh-dependent fluid secretion independent of neurons. (**J**) ΔIsc values of WT pSI and dSI
260 stimulated as indicated. (**K**) Average Isc traces of pSI from WT or *Trpm5*$^{-/-}$ mice stimulated as indicated (5
261 μM C8, basolateral). (**L** and **M**) ΔIsc values of WT tissues compared to (L) tissues from indicated
262 genotypes or (M) tissues pretreated 15 min with atropine (10 μM, basolateral), stimulated as indicated. In
263 the graphs, each symbol represents an individual mouse (one tissue or average of two) pooled from two
264 or more experiments. Groups represent sequential stimulations of the same tissue. *$p < 0.05$, **$p < 0.01$,
265 ***$p < 0.001$, ****$p < 0.001$ by RM one way ANOVA with Tukey's multiple comparisons test (B), two way
266 ANOVA with Dunnett's multiple comparisons test (D, E, L), multiple Mann-Whitney tests with Holm
267 Sídák's multiple comparisons test (C, F, G, H, M). ns, not significant. Graphs depict mean +/- SEM. Also
268 see Figure S2.
269

270 Since enteric neurons are both a major source of ACh and major regulators of
271 fluid secretion in the intestine, we investigated the possibility that SI tuft cells activate
272 enteric neurons. Studies of *Chat*+ tuft cells in the airways have emphasized their close
273 contact with neurons and provided evidence that signaling can occur from tuft cells to
274 neurons, often via release of ACh.[15,16] We therefore looked for similar tuft-neuronal
275 connections by microscopy using the *Chat-GFP* reporter, which marks cholinergic
276 intestinal neurons as well as tuft cells. We found some instances where a GFP+ tuft cell
277 was approached by a GFP+ neuron, but we never saw neurons extend into the
278 epithelium and contact tuft cells, as they do in the airways (Fig. S2D). *Chat*+ neurons
279 represent only a subset of total intestinal neurons,[55] yet staining for the pan-neuronal
280 marker BIII tubulin (TUJ1) revealed no additional neuronal contacts (Fig. S2E),
281 suggesting that neuronal contacts with tuft cells, much less "synapses", are uncommon
282 in the SI.
283 Recognizing that signaling can occur without direct contact, we experimentally
284 tested the requirement for neurons in the succinate response. First, we disrupted
285 neuronal integrity by physically "stripping" the submucosa off the back of the epithelium

286 to eliminate most of the submucosal and all of the myenteric neuronal plexuses[51].
287 Alternatively, we used tetrodotoxin (TTX) to inhibit neuronal action potentials in intact SI
288 tissue[4]. Neither treatment reduced the cESA or CCh responses; in the stripped tissue
289 the CCh response was instead increased, likely due to enhanced diffusion (Fig. 2D).
290 Altogether, our data show that succinate/cESA binds to SUCNR1 expressed apically on
291 epithelial cells and induces chloride-dependent fluid secretion, independently of enteric
292 neurons or submucosal tissue.
293 To confirm that tuft cells were the cells that sensed succinate/cESA to initiate the
294 secretion response, we stimulated dSI from tuft cell-deficient *Pou2f3*$^{-/-}$, and
295 chemosensing-deficient *Trpm5*$^{-/-}$ mice. As with SI tissue from *Sucnr1*$^{-/-}$ mice, tissues
296 from these mice failed to respond to cESA (Fig. 2E). Importantly, the CCh response was
297 intact in all knockout mice, demonstrating that the tissue's capacity for ACh-dependent
298 fluid secretion was unaltered. To test whether ACh was involved in the cESA response,
299 we pretreated the dSI with the pan-mAChR inhibitor atropine and found that this
300 completely blocked the cESA and CCh responses (Fig. 2F). Deletion of *Chat* from IECs
301 using *Chat*$^{fl/fl}$*;Vil1-Cre(Tg+)* mice also abrogated the cESA response (Fig. 2G). Although
302 tuft cells are the only *Chat*-expressing IECs, we also deleted *Chat* in tuft cells
303 specifically using *Chat*$^{fl/fl}$*;Pou2f3*$^{Cre\text{-}ERT2/+}$ mice, and confirmed that tuft cell-derived ACh
304 production was required for cESA-induced fluid secretion (Fig. 2H).
305 Other tuft cell effectors (e.g. LTC_4 or PGD_2) have been implicated acute responses and
306 tuft cells themselves express the receptor for IL-25,[11,56,57] but we excluded the
307 involvement of IL-25 and LTC_4 in ion flux using dSI from *Il25*$^{-/-}$ and *Alox5*$^{fl/fl}$*;Vil1-*
308 *Cre1000(Tg+)* mice, respectively (Fig. S2F,G). Pretreatment with the COX inhibitor
309 ibuprofen to block PGD_2 synthesis also did not affect the cESA response (Fig. S2H).
310 Furthermore, PGD_2, which has not been previously linked with fluid secretion but has
311 been reported to induce mucus secretion from goblet cells (GCs) in the colon[56], did not
312 induce ion flux in the dSI (or the colon) when administered basolaterally (Fig. S2I). We
313 also investigated the possibility that tuft cells were signaling to neighboring cells via gap
314 junctions.[58] The gap junction inhibitor carbenoxolone partially blocked cAMP-driven fluid
315 secretion induced by IBMX + forskolin, but had no effect on cESA or CCh responses
316 (Fig. S2J). Thus, we have demonstrated that tuft cells in the dSI sense lumenal

succinate/cESA and release ACh basolaterally, which stimulates mAChR-dependent Cl^- ion secretion (Fig. 2I). The response is epithelium-intrinsic and does not involve enteric neurons.

Fig. S2: Related to Fig. 2

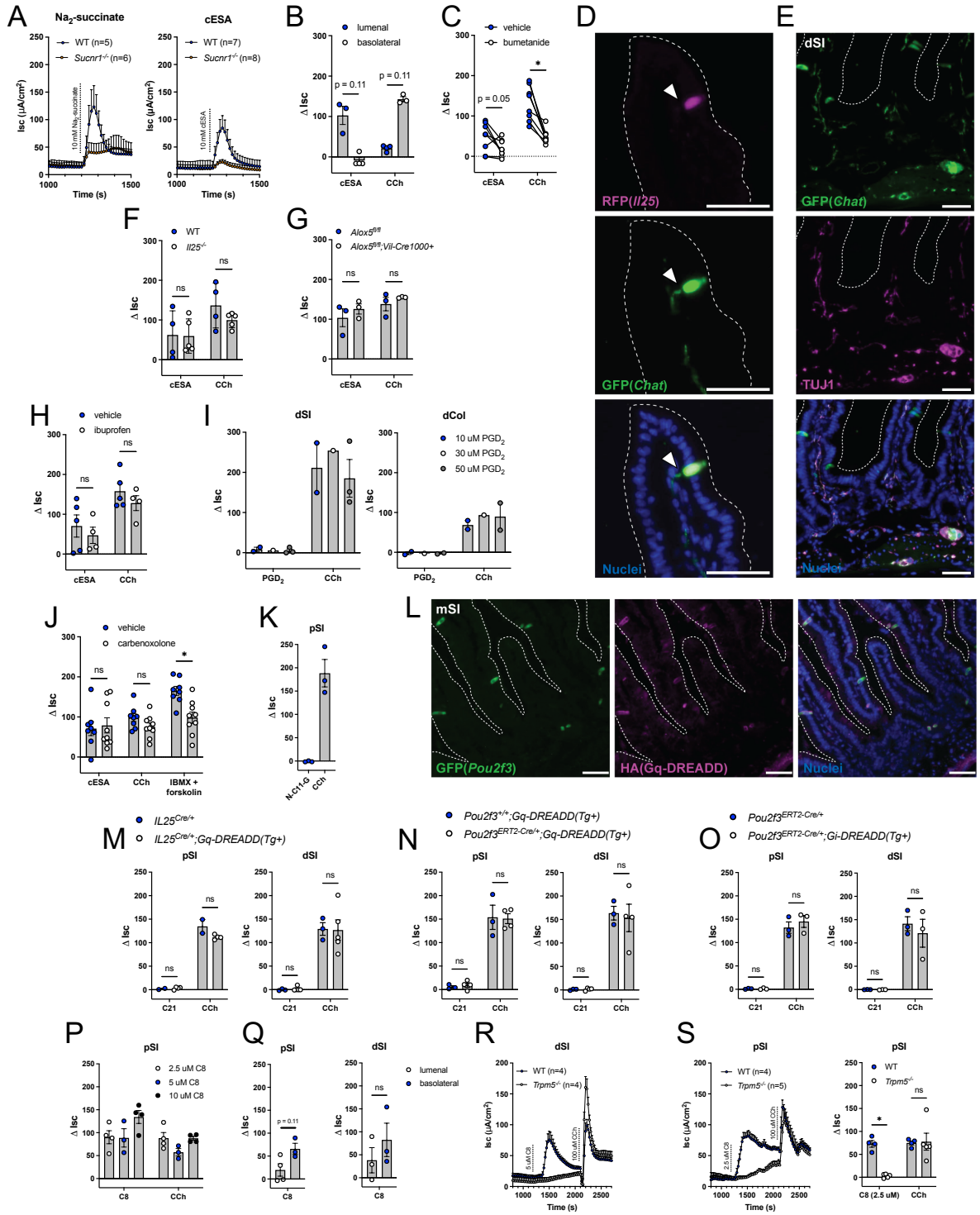

320

321 **Supplemental Figure 2:** (**A**) Average Isc traces of dSI from WT or *Sucnr1*$^{-/-}$ mice stimulated as indicate
322 (Na_2-succinate and cESA, lumenal). (**B**) ΔIsc values of WT dSI stimulated as indicated. (**C**) ΔIsc values of
323 WT dSI pretreated 15 min with vehicle or bumetanide (100 μM, basolateral), stimulated as indicated (10
324 mM cESA lumenal; 100 μM CCh, basolateral). (**D**) Representative immunofluorescence image of a GFP+
325 (green) neuronal process (indicated by solid white arrow) approaching a GFP+/RFP+ (magenta) tuft cell
326 from the dSI of *Chat-GFP*;*Il25*$^{RFP/+}$ mice. Nuclei stained with DAPI (blue). Scale bars: 50 μm. (**E**)
327 Representative immunofluorescence image of GFP+ (green) neurons co-stained for BIII tubulin (TUJ1,
328 magenta) in the dSI. Nuclei stained with DAPI (blue). Scale bars: 50 μm. (**F**, **G**, and **H**) (F and G) ΔIsc
329 values of dSI from indicated genotypes or (H) WT dSI compared to dSI pretreated 15 min with ibuprofen
330 (10 μM, bilateral), stimulated as indicated. (**I**) ΔIsc values of WT tissues stimulated as indicated (PGD_2,
331 basolateral). (**J**) ΔIsc values for WT dSI compared to dSI pretreated 15 min with carbenoxolone (1 mM,
332 lumenal), stimulated as indicated (100 μM IBMX + 10 μM forskolin, bilateral). (**K**) ΔIsc values of WT pSI
333 stimulated as indicated (100 μM N-C11-G, lumenal). (**L**) Representative immunofluorescence image of
334 GFP+ (green) tuft cells expressing HA+ Gq-DREADDs (magenta) in the crypts and villi of the medial SI
335 (mSI). Nuclei stained with DAPI (blue). Scale bars: 50 μm. (**M**, **N**, and **O**) (M) ΔIsc values of indicated
336 tissues from unmanipulated mice or (N and O) indicated tissues from mice 7 days after start of tamoxifen
337 chow, stimulated as indicated (1 μM C21, bilateral). (**P**) ΔIsc values of WT pSI stimulated as indicated
338 (C8, bilateral). (**Q**) ΔIsc values of WT tissues from pSI and dSI stimulated as indicated. (**R**) Average Isc
339 traces of dSI stimulated as indicated (5 μM C8, basolateral). (**S**) Average Isc traces and ΔIsc values of
340 pSI stimulated as indicated (2.5 μM C8, basolateral). In the graphs, each symbol represents an individual
341 mouse (one tissue or average of two) pooled from two or more experiments. Groups represent sequential
342 stimulations of the same tissue. In (C) paired vehicle and bumetanide-treated tissues are from the same
343 mouse. *$p < 0.05$, **$p < 0.01$, ***$p < 0.001$, ****$p < 0.001$ by multiple Mann-Whitney tests with Holm
344 Sídák's multiple comparisons test (B, F-H, J, M-O, S), Wilcoxon matched-pairs signed rank test with Holm
345 Sídák's multiple comparisons test (C), or Mann-Whitney test (Q). ns, not significant. Graphs depict mean
346 +/- SEM.

347

348 ***A TRPM5 agonist induces tuft- and ACh-dependent fluid secretion in the pSI and***
349 ***dSI***

350 In characterizing the succinate response, we found that the pSI did not respond
351 to succinate stimulation (Fig. 2J). This finding is consistent with greater succinate
352 receptor (*Sucnr1*) expression in tuft cells from the dSI compared to the pSI (Table S2),[23]
353 and may also reflect the reduced frequency of *Chat*+ tuft cells in the pSI (Fig. 1D). Since
354 the pSI was responsive to CCh, we reasoned that pSI tuft cells could induce fluid

355 secretion if properly stimulated. We first tested several putative tuft cell ligands. Worm
356 excretory and secretory products from *Nippostrongylus brasiliensis* (*Nb*), known as
357 NES, failed to stimulate ion flux whether made from infective L3 larvae or adult worms
358 (data not shown). The bacterial metabolite N-C11-G did not induce ion flux either (Fig.
359 S2K). Next, we tried a chemogenetic approach with Gq- or Gi-coupled receptors that
360 respond only to synthetic ligands (DREADDs)[59] using constitutive (*Il25-Cre*) or inducible
361 (*Pou2f3*$^{Cre\text{-}ERT2/+}$) for tuft cell-specific expression. Although tuft cells expressed the HA
362 tag included in the DREADD constructs, stimulation with Compound 21[60] was
363 insufficient to drive a fluid secretion response in the pSI or dSI (Fig. S2L-O). Perhaps G
364 proteins required for DREADD function are not available in tuft cells or the signals
365 induced downstream of DREADD activation are not sufficient to induce ACh release.
366 Finally, we decided to stimulate TRPM5 directly, since all tuft cell chemosensing
367 pathways identified to date converge on TRPM5. We acquired a TRPM5 agonist
368 compound called Class 8 (C8),[61,62] and found that it induced ion flux in both the pSI and
369 dSI when administered lumenally or basolaterally, with a trend toward higher basolateral
370 responses (Fig. 2K, S2P-Q). The C8 response was similar to cESA- or CCh-induced ion
371 flux, and was TRPM5-dependent in the pSI and dSI (Fig. 2K-L, S2R). The C8 response
372 was also tuft cell- and ACh-dependent in both locations (Fig. 2L-M). In the pSI, C8
373 induced a slow TRPM5-independent increase in Isc (Fig. 2K), but this off-target effect
374 could be eliminated by lowering the dose of C8 (Fig. S2S). We conclude that in
375 response to direct TRPM5 activation, tuft cells in the pSI and dSI can release ACh to
376 induce fluid secretion from the intestinal epithelium.
377
378 ***Tuft cell-mediated fluid secretion occurs across mucosal tissues and is***
379 ***detectable in vivo***
380 We previously found that *Sucnr1* expression is even higher in tracheal tuft cells
381 than those of the SI,[11] so to test if tuft cells regulate fluid secretion at multiple mucosal
382 barriers, we stimulated tracheal tissue in the Ussing chamber with succinate. As in the
383 dSI, we found that this induced a rapid increase in the Isc that was *Pou2f3*-, *Sucnr1*-,
384 and *Trpm5*-dependent (Fig. 3A-B). In addition, the response was mAChR-dependent
385 (Fig. 3C). By comparison, the cecum and colon, where tuft cells express *Sucnr1* at low

386 levels,[11] responded only weakly to succinate stimulation and in a tuft-independent
387 manner (Fig. S3A). Colonic tissue did respond to TRPM5 agonism with C8, with a larger
388 response in the proximal colon (pCol) than the distal colon (dCol) (Fig. 3D-E) (ref.). The
389 reported tuft ligand N-C11-G[56] did not stimulate fluid secretion from the dSI or dCol (Fig.
390 S3B), and also failed to elicit tuft-dependent leukotriene production from intestinal
391 epithelial monolayers (Fig. S3C). Therefore, tuft cell control of epithelial fluid secretion is
392 a common effector function across barrier tissues.
393 The Ussing chamber measures ion flux but cannot measure water movement
394 directly. We therefore wanted to test if activating tuft cells *in vivo* could induce fluid
395 secretion into the intestine. We dosed mice with C8 or vehicle in the morning and then
396 measured the wet weight of fecal pellets 3 hours later. In mice given vehicle, the fecal
397 water content declined, likely due to reduced water intake during the day. C8 treatment
398 prevented this decline, indicating sustained fluid secretion (Fig. 3F). Importantly, this
399 fluid secretion was dependent on epithelial *Chat* (Fig. 3G, S3D). Thus, activation of tuft
400 cells along the intestinal tract induces ACh-dependent ion flux that drives fluid secretion
401 into the intestinal lumen.

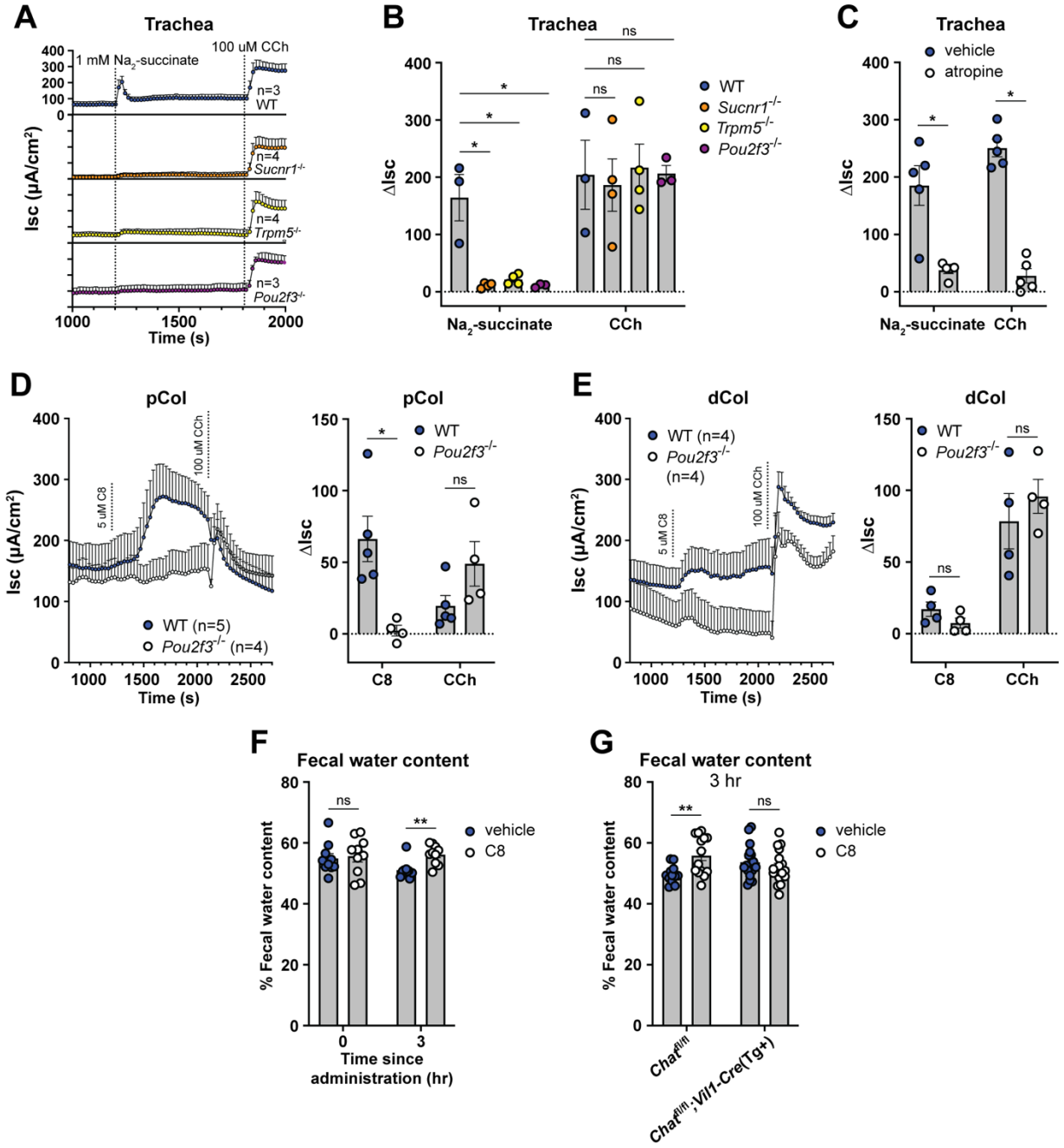

Figure 3: ***Tuft cell-mediated fluid secretion occurs across mucosal tissues and is detectable in vivo.*** (**A** and **B**) (A) Average Isc traces and (B) ΔIsc values of trachea from mice of indicated genotypes stimulated as indicated (1 mM Na_2-succinate, lumenal; 100 µM CCh, basolateral). (**C**) ΔIsc values of WT trachea compared to trachea pretreated 15 min with atropine (10 µM, basolateral), stimulated as indicated. (**D** and **E**) Average Isc traces and ΔIsc values of WT and *Pou2f3*$^{-/-}$ tissues stimulated as indicated (5 µM C8, basolateral). (**F** and **G**) Quantification of water content of fecal pellets collected from (A) WT or (B) *Chat-fl;Vil1-Cre(Tg+)* mice treated orally with vehicle or C8 (30 mg/kg) for the indicated durations. In the graphs, each symbol represents an individual mouse (one tissue or average of two)

411 pooled from two or more experiments. Groups represent sequential stimulations or timepoints of the same
412 tissue or animal. *p < 0.05, **p < 0.01, ***p < 0.001, ****p < 0.001 by, two way ANOVA with Tukey's
413 multiple comparisons test (B), or multiple Mann-Whitney tests with Holm Sídák's multiple comparisons
414 test (C-G). ns, not significant. Graphs depict mean +/- SEM. Also see Figure S3.
415

Fig. S3: Related to Fig. 3

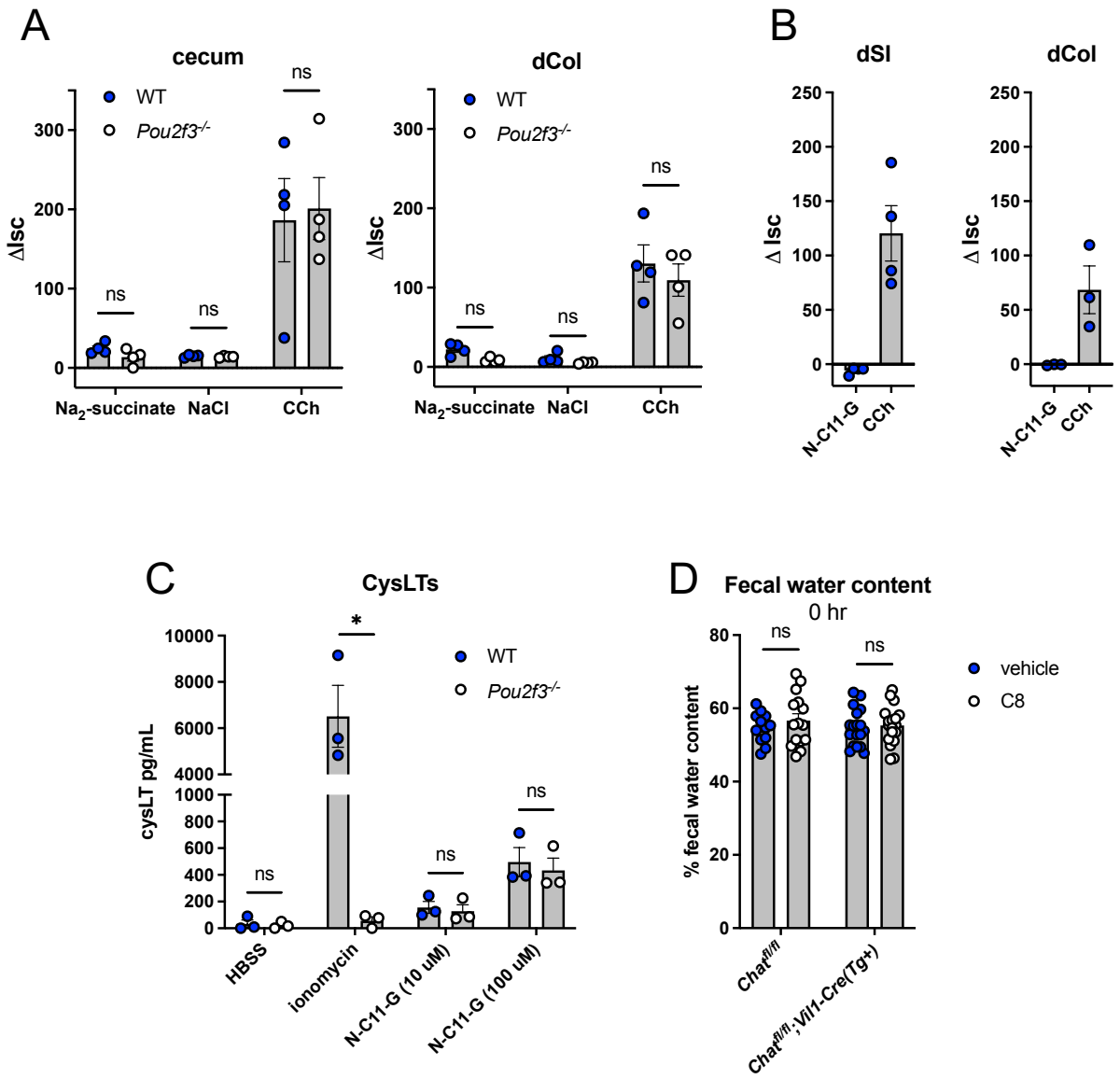

416

417 **Supplemental Figure 3:** (**A**) ΔIsc values of WT and *Pou2f3*$^{-/-}$ tissues stimulated as indicated (10 mM Na_2-
418 succinate and 20 mM NaCl, lumenal; 100 μM CCh, basolateral). (**B**) ΔIsc values of WT tissues stimulated
419 as indicated (100 μM N-C11-G, lumenal). (**C**) Cysteinyl leukotriene (CysLTs) production from WT and

420 *Pou2f3*$^{-/-}$ SI epithelial monolayers stimulated as indicated. (**D**) Quantification of water content of fecal
421 pellets collected from indicated mice immediately after oral treatment with C8 (30 mg/kg). In the graphs,
422 each symbol represents an individual mouse pooled from two or more experiments. In (A-B) groups
423 represent sequential stimulations of the same tissue and in (C) groups represent individual monolayers.
424 *p < 0.05, **p < 0.01, ***p < 0.001, ****p < 0.001 by multiple Mann-Whitney tests with Holm Sídák's
425 multiple comparisons test (A, D), or multiple unpaired t tests with Holm Sídák's multiple comparisons test
426 (C). ns, not significant. Graphs depict mean +/- SEM.
427

428 ***Tuft cell-derived ACh is not required for ILC2 activation***

429 Having defined ACh-dependent fluid secretion as a tuft cell effector function in
430 unmanipulated mice, we next considered the role of tuft cell-derived ACh during Type 2
431 immunity. Consistent with previous reports in the airways,[63] we found that tamoxifen
432 partially suppressed Type 2 responses in the intestine. For example, treating protist-
433 colonized *Chat*$^{fl/fl}$*;Pou2f3*$^{Cre\text{-}Ert2/+}$ mice with tamoxifen for one week reduced tuft cell
434 counts by nearly half in both WT and Cre+ mice (Fig. S4A). The effect of tamoxifen was
435 less noticeable during helminth infection, perhaps because this induces more Type 2
436 inflammation (Fig. S4B). Nonetheless, given these non-specific effects of tamoxifen, we
437 focused on identifying *Chat*-dependent effects by analyzing *Chat*-sufficient and *Chat*-
438 deficient mice that had all been treated with tamoxifen.

439 Previously characterized SI tuft cell effector molecules (e.g. IL-25 and LTC_4)
440 have primarily been shown to regulate ILC2 activation.[21,27] Also, recent studies have
441 reported that ILC2s express *Chat* following activation and that ACh can potentiate their
442 production of cytokines and proliferation, perhaps via autocrine signaling[64,65]. We
443 therefore asked if tuft cell-derived ACh was signaling to ILC2s in addition to inducing
444 fluid secretion. We began by testing if ACh could enhance ILC2 activation using an *in*
445 *vitro* model of acute (6-hour) ILC2 stimulation.[27] Pairing ACh with IL-25 to mimic the
446 results of tuft cell activation, we failed to detect any ACh-dependent ILC2 activation as
447 measured by IL-13 reporter expression and secretion of IL-13 and IL-5 (Fig. S4C-D). By
448 contrast, LTC_4 greatly enhanced ILC2 activation when given with IL-25, as expected.
449 We conclude that ACh does not induce cytokine expression in ILC2s sorted from
450 unmanipulated mice and is therefore unlikely to contribute to their initial activation.
451

Fig. S4: Related to Fig. 4

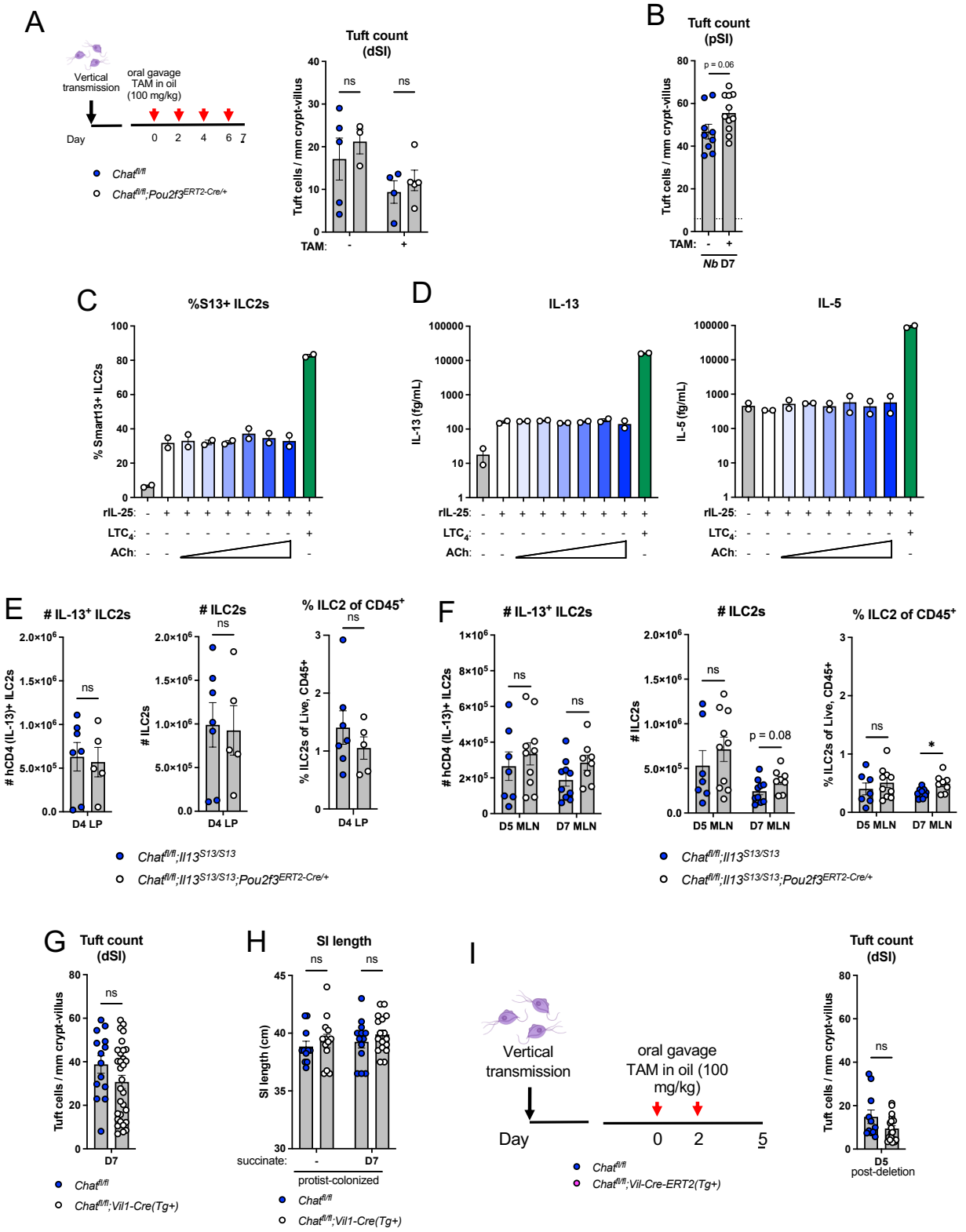

453 **Supplemental Figure 4:** (**A**) Schematic of tamoxifen (TAM) treatment of protist-colonized *Chat-fl;*
454 *Pou2f3*$^{ERT2\text{-}Cre/+}$ mice and quantification of dSI tuft counts by immunofluorescence at D7 after start of
455 treatment. (**B**) Quantification of pSI tuft counts by immunofluorescence of WT mice treated with or without
456 tamoxifen and infected with *Nb* for 7 days. (**C** and **D**) (C) Flow cytometric quantification of percent hCD4+
457 (IL-13+) SILP ILC2s and (D) IL-13 and IL-5 concentration in their supernatant after 6 hr *in vitro* culture
458 with the indicated conditions (0.1 ng/mL rIL-25, serial 10-fold dilutions of ACh from 10 mM to 0.1 μM, 1
459 nM LTC_4). (**E** and **F**) Quantification of number of hCD4+ (IL-13+) ILC2s, total ILC2s, and percent ILC2s at
460 the indicated timepoints, tissues, and genotypes. (**G**) Quantification of dSI tuft counts by
461 immunofluorescence from indicated mice treated with 150 mM succinate drinking water for 7 days. (**H**) SI
462 length from indicated mice vertically-colonized with *T. rainier* protists with or without 7 days of additional
463 150 mM succinate drinking water treatment. (**I**) Schematic of acute deletion of *Chat* from vertically *T.*
464 *musculis* (*Tm*) -colonized mice and quantification of dSI tuft counts by immunofluorescence 5 days after
465 start of treatment. In the (A-B, E-I), each symbol represents an individual mouse from two or more pooled
466 experiments. In (C and D) each symbol represents a technical replicate of cells sorted from pooled mice.
467 *p < 0.05, **p < 0.01, ***p < 0.001, ****p < 0.001 by multiple Mann-Whitney tests with Holm Sídák's
468 multiple comparisons test (A, F, H) or Mann-Whitney test (B, E, G, I). ns, not significant. Graphs depict
469 mean +/- SEM.
470
471 To test if tuft cell-derived ACh was involved in ILC2 activation *in vivo* and at later
472 timepoints, we generated *Chat*$^{fl/fl}$*;Pou2f3*$^{ERT2\text{-}Cre/+}$ mice that also expressed an IL-13
473 reporter (Smart13). We treated these mice with tamoxifen, infected with *Nb*, and
474 assessed early ILC2 activation in the LP 4 days post infection (dpi), about 2 days after
475 the worms arrive in the intestine. We found no difference in ILC2 activation or expansion
476 (Fig. 4A, S4E). Since *Chat* has been detected in activated but not resting ILC2s, we
477 also tested if tuft cell-derived ACh regulated ILC2s later during infection. Given the
478 difficulty of isolating viable cells from Type 2 inflamed SI, we assessed ILC2s in the
479 mesenteric lymph nodes at 5 and 7 dpi. Again, we saw equivalent activation and
480 expansion of ILC2s between *Chat*-sufficient and -deficient mice (Fig. 4B, S4F). We
481 conclude that tuft cell-derived ACh does not contribute to ILC2 activation during
482 helminth infection of the SI.
483
484 ***Tuft cell-derived ACh is not required for Type 2 intestinal remodeling***
485 An effective immune response to helminths requires intestinal remodeling, such
486 as hyperplasia of tuft cells and mucus-producing GCs and lengthening of the SI.[23,66] IL-

487 13 is critical for this process, but ACh might also contribute. For example, ACh has been
488 implicated in direct modulation of epithelial cell differentiation,[67,68] and could also impact
489 tissue remodeling via other AChR-expressing cells, such as neurons.[55]
490 Using tuft cell frequency, goblet cell frequency, and intestinal length as markers
491 of SI remodeling, we found little or no defect 7 days after *Nb* infection of mice with either
492 constitutive (*Vil1-Cre(Tg+)*) or acute (*Vil1-Cre-Ert2(Tg+)*) deletion of *Chat* in IECs (Fig.
493 4C-E). The same was true both 5 and 7 days after *Nb* infection when we used *Pou2f3-*
494 *Cre-ERT2* for tuft cell-specific *Chat* deletion (Fig. 4F-H). Since tuft cell circuits are
495 distinct in the pSI and dSI,[11,27] we also tested Type 2 remodeling in the dSI 4 and 7
496 days after starting treatment with succinate-supplemented drinking water. As before,
497 there was little effect of either constitutive or inducible IEC *Chat* deletion (Fig. 4I-K;
498 S4G). Likewise, *Chat*$^{fl/fl}$*;Vil1-Cre(Tg+)* mice vertically colonized with protists had no
499 defect in tuft cell hyperplasia or SI length at homeostasis or following one week of
500 additional succinate drinking water treatment (Fig. 4L, S4H). Acute loss of *Chat* in
501 protist-colonized *Chat*$^{fl/fl}$*;Vil1-Cre-ERT2(Tg+)* mice also had no effect on tuft cell
502 hyperplasia 5 days later (Fig. S4I). In sum, Type 2 remodeling is broadly intact in the
503 absence of tuft cell ACh. We did observe small but significant decreases in tuft cell
504 hyperplasia or SI lengthening in some assays, but this effect was inconsistent and
505 minimal compared to loss of other tuft cell effector molecules (e.g. IL-25 and LTC_4).[21,27]
506
507

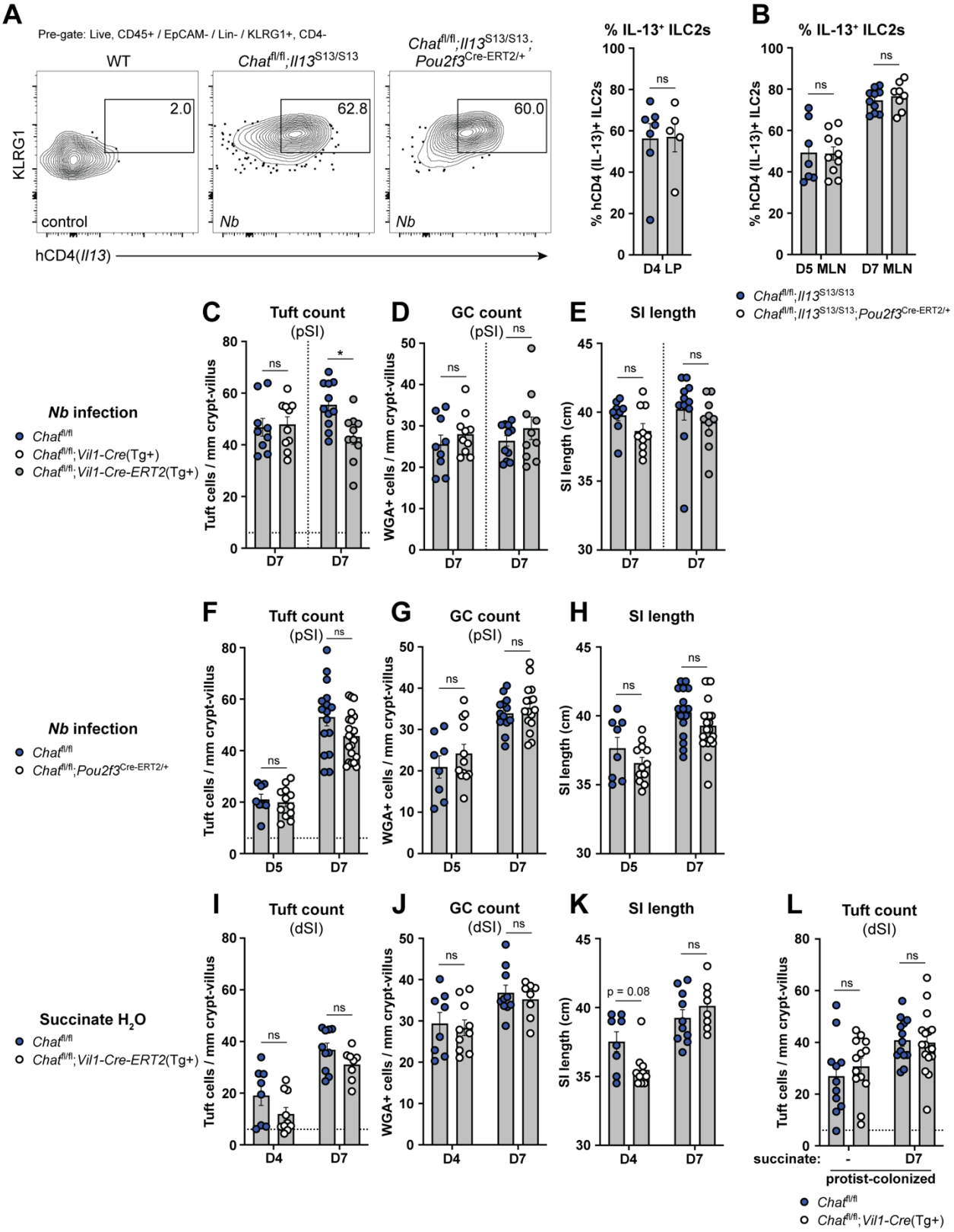

508

509 **Figure 4: Tuft cell-derived ACh is not required for ILC2 activation or intestinal remodeling.** (**A** and

510 **B**) (A) Representative flow cytometry and quantification of percent hCD4$^+$ (IL-13$^+$) ILC2s (Lin$^-$, CD45$^+$,

511 KLRG1^{+}, CD4^{-}) in the SI LP and (B) mesenteric lymph nodes (MLN) at the indicated *Nb* infection
512 timepoints. (**C**, **D**, and **E**) (C) Quantification of pSI tuft cells (DCLK1+) and (D) goblet cells (WGA+) by
513 immunofluorescence and (E) total SI length from the indicated mice at D7 of *Nb* infection. (**F**, **G**, and **H**)
514 Same analysis as in C-E in the indicated mice at the indicated *Nb* infection timepoints. (**I**, **J**, and **K**) Same
515 analysis as in C-E in the indicated mice at the indicated timepoints of 150 mM succinate drinking water
516 treatment. (**L**) Quantification of tuft cells (DCLK1+) by immunofluorescence from indicated mice vertically-
517 colonized with *T. rainier* protists with or without 7 days of additional 150 mM succinate drinking water
518 treatment. In the graphs, each symbol represents an individual mouse from two or more pooled
519 experiments. For graphs of tuft cell counts, horizontal dashed line signifies baseline tuft cell count in
520 unmanipulated mice. *$p < 0.05$, **$p < 0.01$, ***$p < 0.001$, ****$p < 0.001$ by Mann Whitney test (A) or
521 multiple Mann-Whitney tests with Holm Sídák's multiple comparisons test (B-L). ns, not significant.
522 Graphs depict mean +/- SEM. Also see Fig. S4.
523

524 ***Tuft cell hyperplasia results in enhanced ACh-dependent fluid secretion***

525 The ability of tuft cells to induce fluid secretion in the steady state led us to ask
526 how it would change during Type 2 inflammation, when tuft cell numbers can increase
527 10-fold and fluid secretion might support worm clearance as part of the canonical weep
528 and sweep response. First, we asked whether the number and frequency of *Chat*+ tuft
529 cells changed with Type 2 inflammation. While the frequency of *Chat*+ tuft cells
530 decreased (Fig. S5A), this was more than compensated for by the hyperplasia, such
531 that the total number of *Chat*+ tuft cells per millimeter crypt/villus was increased in the
532 pSI and especially the dSI 7 days after either succinate-treatment or *Nb*-infection (Fig.
533 5A).

534 Next, we infected mice with *Nb* to induce tuft cell hyperplasia and quantified the
535 fluid secretion response to succinate in the pSI and dSI across the course of infection.
536 Although pSI tuft cells do not respond to succinate at steady state, we wondered if
537 those that emerge during infection might be responsive. The pSI did not become
538 responsive to succinate (or cESA) over the course of infection, but the dSI succinate
539 response increased by day 7, when tuft cell numbers peaked (Fig. 5B, S5B-C). The
540 increased response to succinate was less than the ~3-fold increase of *Chat*+ tuft cells
541 that we observed on D7 of *Nb* infection, likely because the epithelium's total capacity to
542 respond to ACh/CCh was reduced by Type 2 inflammation, as previously reported (Fig.
543 5B).[69]

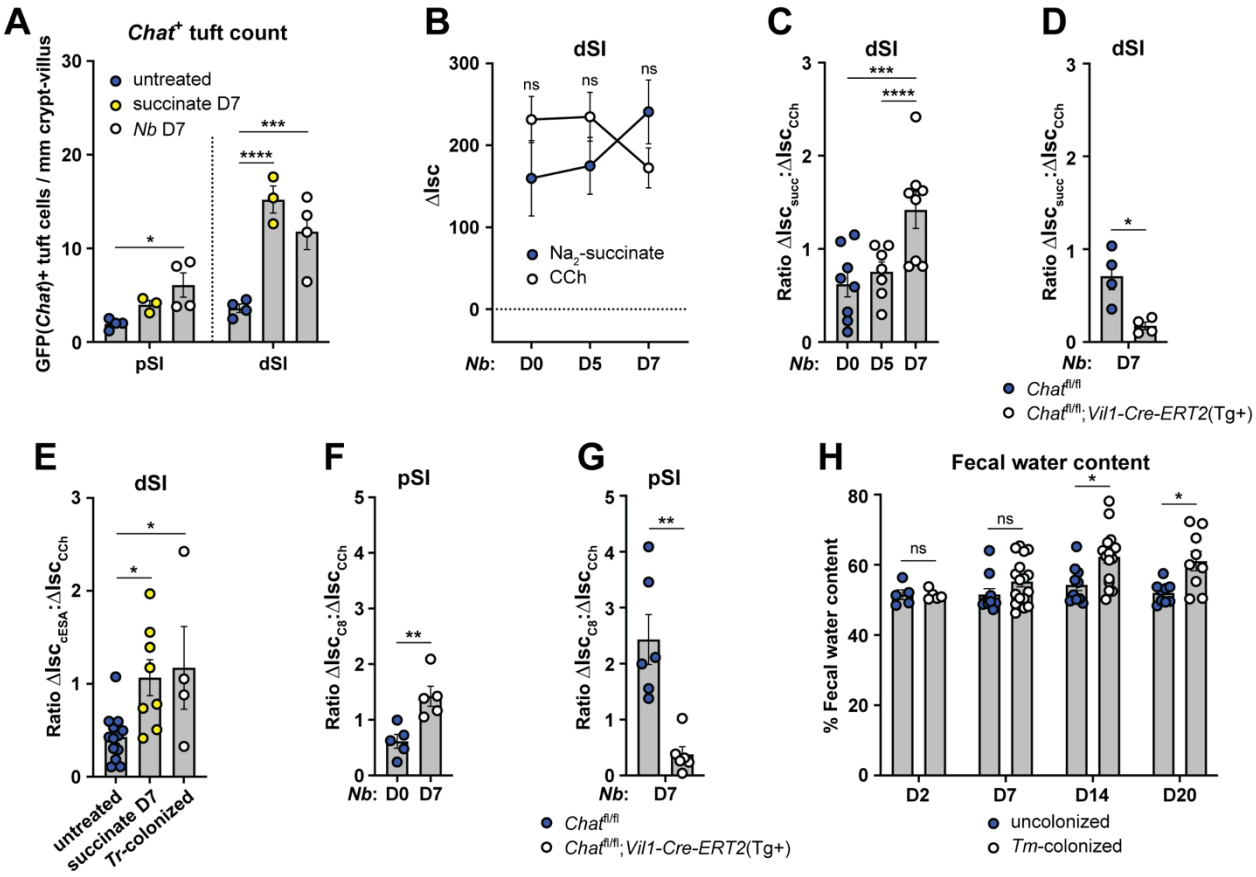

Figure 5: Tuft cell hyperplasia results in enhanced ACh-dependent fluid secretion. (**A**) Quantification of GFP(*Chat*)+ tuft cells (*Il25*-RFP+) from the pSI and dSI of WT mice untreated, treated with 150 mM Na_2-succinate drinking water (succinate), or infected with *N. brasiliensis* (*Nb*) for 7 days. (**B**) ΔIsc values of dSI from WT mice infected with *Nb* for the indicated number of days and stimulated as indicated (10 mM succinate, lumenal; 100 μM CCh, basolateral). (**C**) Ratio of succinate ΔIsc values to CCh ΔIsc values of dSI from (B). (**D**) Ratio of succinate ΔIsc values to CCh ΔIsc values of dSI of indicated mice 7 days after *Nb* infection. (**E**) Ratio of cESA ΔIsc values to CCh ΔIsc values of dSI from WT mice treated with succinate (as in A) or vertically colonized with *T. rainier* (*Tr*) protists. (**F** and **G**) Ratio of C8 ΔIsc values to CCh ΔIsc values of pSI from (F) WT or (G) mice of indicated genotypes mice at indicated timepoints after *Nb* infection. (**H**) Quantification of water content of fecal pellets collected at indicated timepoints post *T. musculis* (*Tm*) colonization of WT mice. In the graphs, each symbol represents an individual mouse pooled from two or more experiments. *p < 0.05, **p < 0.01, ***p < 0.001, ****p < 0.001 by two way ANOVA with Dunnett's multiple comparisons test (A), Mann-Whitney test (B, D, F-G), one way ANOVA (C, E), or multiple Mann-Whitney tests with Holm Sídák's multiple comparisons test (H). ns, not significant. Graphs depict mean +/- SEM. Also see Fig. S5.

561 This effect could be quantified by measuring the ratio of succinate-induced ΔIsc to CCh-
562 induced ΔIsc (Fig. 5C), highlighting how hyperplasia allows tuft cells to capture a greater
563 proportion of the total epithelial ACh response. We confirmed that the increased
564 succinate response on day 7 still required epithelium-derived ACh (Fig. 5D, S5D) and
565 did not occur without *Sucnr1* (Fig. S5E). Enhanced succinate/cESA-induced fluid
566 secretion was also observed if tuft cell hyperplasia was established with oral succinate
567 or *Tritrichomonas* colonization (Fig. 5E). We found that tuft cell hyperplasia induced by
568 *Nb* infection also increased C8-dependent fluid secretion in both the pSI and dSI, and
569 that this required epithelial *Chat* (Fig. 5F-G, S5F-K).
570 To further test the hypothesis that increased numbers of tuft cells drive increased
571 succinate-induced fluid secretion during Type 2 remodeling, we turned to Balb/c mice.
572 Unmanipulated Balb/c mice are nearly tuft cell-deficient in the dSI, but activation of
573 ILC2s with exogenous IL-25 increases tuft cell numbers (Fig. S5L).[44] Accordingly,
574 unmanipulated Balb/c dSI did not respond to cESA in the Ussing chamber, but
575 responsiveness was induced by rIL-25 treatment, indicating that increased numbers of
576 ACh-producing tuft cells were needed (Fig. S5M).
577 Lastly, to test if *in vivo* fluid secretion was enhanced during Type 2 remodeling,
578 we measured the fecal water content of protist-colonized mice. Compared to
579 uncolonized mice, mice colonized with the succinate-producing protist *T. musculis* had
580 increased fecal water content by 14 and 20 days after colonization (Fig. 5H). This
581 suggested that tuft cells were repeatedly responding to protist-derived succinate and
582 inducing fluid secretion. Thus, the increased number of *Chat*+ tuft cells induced during
583 SI Type 2 inflammation drives increased ACh-dependent fluid secretion despite an
584 overall desensitization of the tissue to ACh.

Fig. S5: Related to Fig. 5

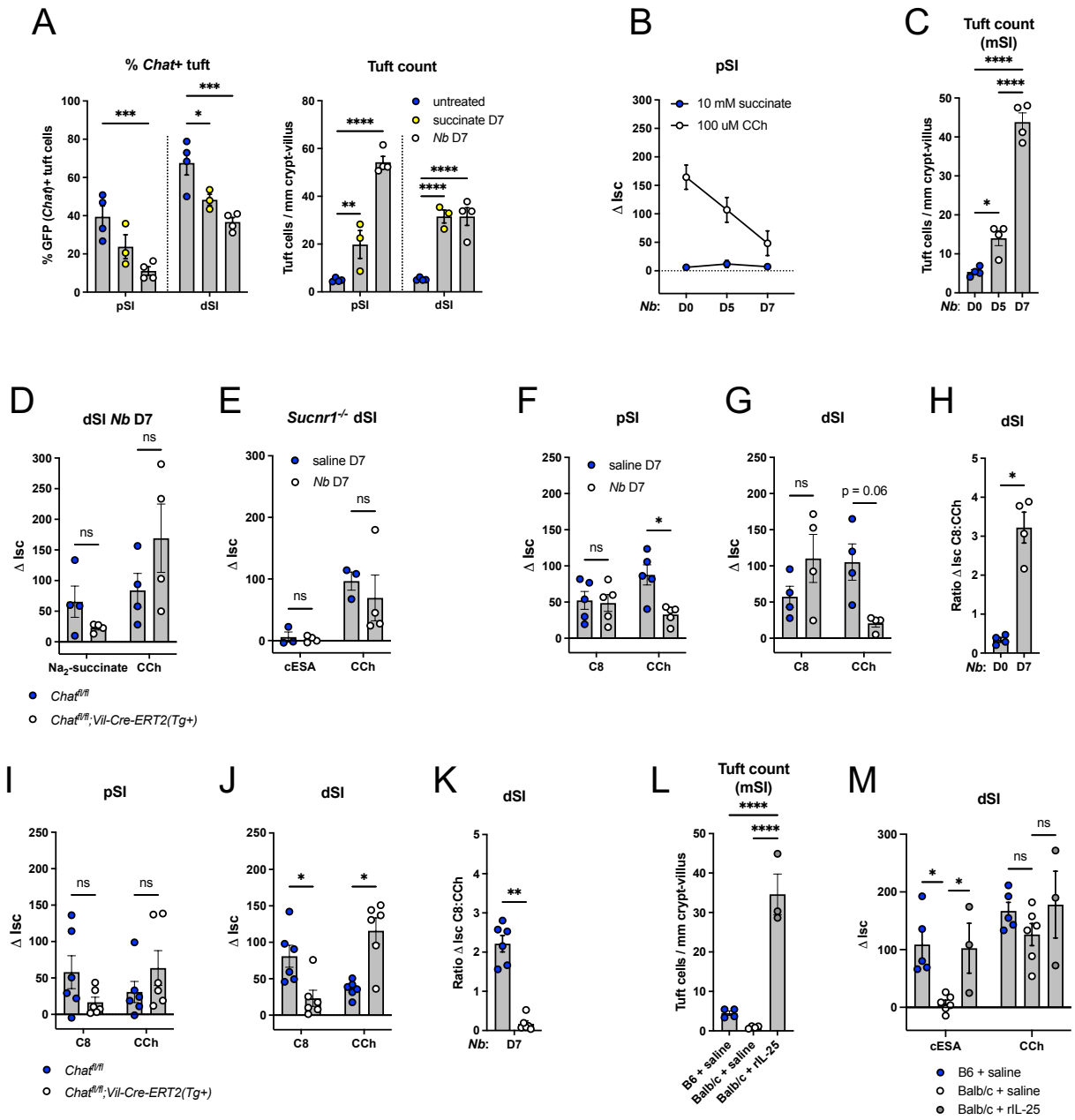

Supplemental Figure 5: (**A**) Quantification of percent GFP(*Chat*)+ tuft cells and RFP(*Il25*)+ tuft cells from the pSI and dSI of WT mice untreated, treated with 150 mM Na_2-succinate drinking water (succinate), or infected with *N. brasiliensis* (*Nb*) for the duration indicated. (**B**) ΔIsc values of pSI from WT mice infected with *Nb* for the indicated number of days and stimulated as indicated (10 mM succinate, lumenal; 100 μM CCh, basolateral). (**C**) Quantification of tuft cells (DCLK1+) by immunofluorescence from medial SI (mSI) of mice in (B). (**D**) ΔIsc values of dSI from mice of indicated genotypes infected with *Nb* for 7 days and stimulated as indicated. (**E**) ΔIsc values of *Sucnr1*$^{-/-}$ dSI with or without 7 day *Nb* infection, stimulated as

593 indicated. (**F-G**) ΔIsc values of (F) pSI and (G) dSI from WT mice with or without 7 day *Nb* infection,
594 stimulated as indicated. (**H**) Ratio of C8 ΔIsc values to CCh ΔIsc values in (G). (**I** and **J**) ΔIsc values of (I)
595 pSI and (J) dSI from mice of indicated genotype infected with *Nb* for 7 days, stimulated as indicated. (**K**)
596 Ratio of C8 ΔIsc values to CCh ΔIsc values from (J). (**L**) Quantification of tuft cells (DCLK1+) by
597 immunofluorescence in the mSI of mice of indicated genotypes treated as indicated. (**M**) ΔIsc values of
598 dSI from mice in (L) stimulated as indicated. In the graphs, each symbol represents an individual mouse
599 (one tissue or average of two) from two or more pooled experiments. *$p < 0.05$, **$p < 0.01$, ***$p < 0.001$,
600 ****$p < 0.001$ by two way ANOVA with Dunnett's multiple comparisons test (A) two way ANOVA with
601 Tukey's multiple comparisons test (M), Mann-Whitney test (B, H, K), one way ANOVA with Tukey's
602 multiple comparisons test (C, L), or multiple Mann-Whitney tests with Holm Sídák's multiple comparisons
603 test (D-G, I-J). ns, not significant. Graphs depict mean +/- SEM.
604

605 ***Tuft cell ACh regulates helminth clearance but not protist colonization***

606 There is little evidence to suggest that tuft cell sensing of *Tritrichomonas sp.* and
607 the resulting Type 2 immune response in the SI alter the total abundance of protists,[22]
608 but we wondered if tuft cell induced fluid secretion might instead regulate protist
609 localization along the length of the SI, with the goal of containing protists to the dSI and
610 cecum. We therefore assessed the abundance of protists across the pSI, dSI, and
611 cecum of vertically-colonized *Chat*$^{fl/fl}$*;Vil1-Cre* mice (Fig. S5M-N), hypothesizing an
612 increase of protists in the pSI of *Chat*-deficient mice. Constitutive deletion of *Chat* in tuft
613 cells had no effect on protist abundance or localization across the SI or cecum (Fig.
614 S5N). Treating protist-colonized mice with succinate to amplify Type 2 immunity also did
615 not uncover a phenotype (Fig. S5N), and acute deletion of *Chat* for 5 days likewise
616 failed to alter protist abundance or localization (Fig. S5O). Thus, the physiologic function
617 of protist sensing by tuft cells remains unclear.

Fig. S6: Related to Fig. 6

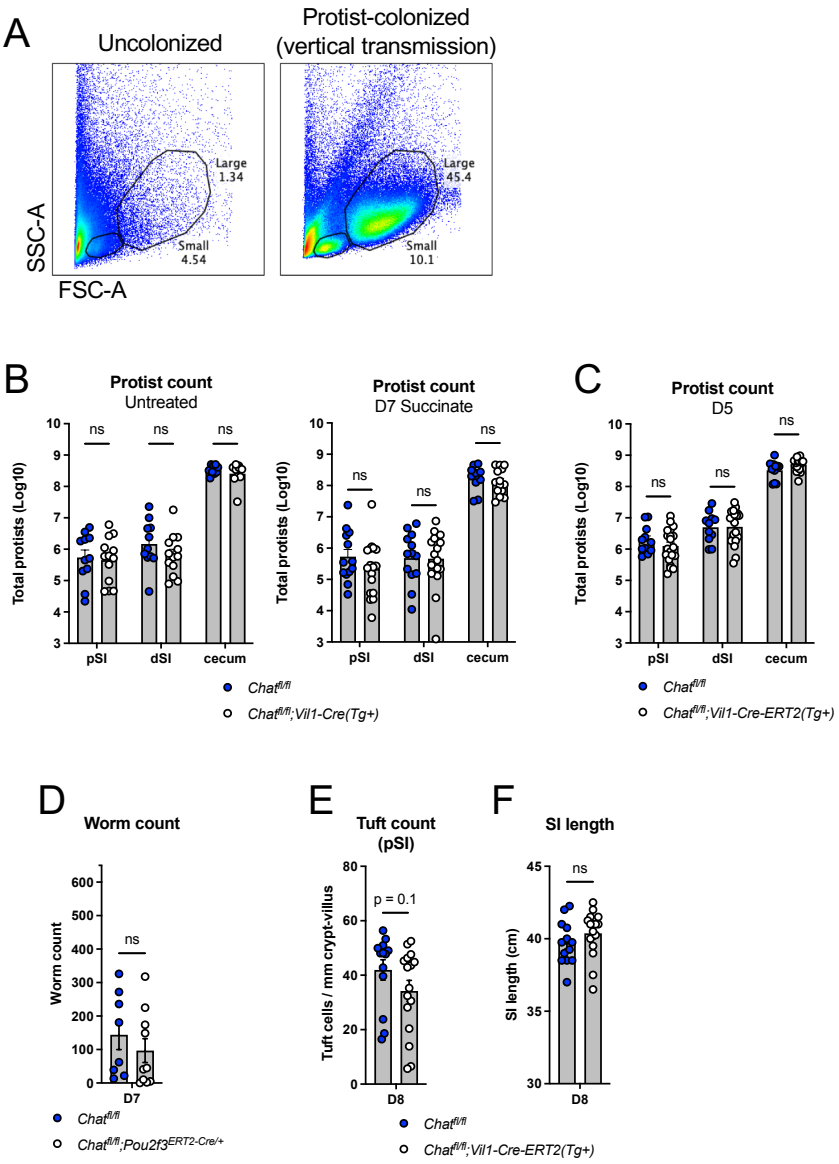

Supplemental Figure 6: (**A**) Representative flow cytometry of cecal contents from uncolonized and protist-colonized mice showing gating of protists by size. (**B**) Quantification of total protists by flow cytometry in indicated tissues of vertically-colonized mice of indicated genotypes left untreated or given 150 mM Na_2-succinate in drinking water for 7 days. (**C**) Quantification of total protists by flow cytometry in indicated tissues of vertically-colonized mice of indicated genotypes administered tamoxifen 5 days prior to analysis. (**D**) Quantification of total SI *Nb* in mice of indicated genotype infected with *Nb* for 7 days without tamoxifen administration. (**E** and **F**) (E) Quantification of tuft cells (DCLK1+) by immunofluorescence and (F) total SI length 8 days post *Nb* infection of mice of indicated genotype given a single dose of tamoxifen (125 mg/kg) on day 5. In the graphs, each symbol represents an individual

627 mouse (one tissue or average of two) from two or more pooled experiments. *p < 0.05, **p < 0.01, ***p <
628 0.001, ****p < 0.001 by multiple Mann-Whitney tests with Holm Sídák's multiple comparisons test (B-C) or
629 Mann-Whitney test (D-F). ns, not significant. Graphs depict mean +/- SEM.
630
631 On the other hand, the requirement for tuft cell sensing and downstream Type 2
632 immunity for clearing helminths from the SI is well established.[11,20,45] To test if tuft cell
633 ACh contributes to helminth clearance, despite not impacting ILC2 activation or tissue
634 remodeling, we assessed worm burden in mice lacking epithelial *Chat* at 7 dpi, a
635 timepoint when WT mice begin to clear worms from the SI. Indeed, both constitutive and
636 acute deletion of epithelial *Chat* led to an increased SI worm burden (Fig. 5I). Tuft-
637 specific *Chat* deletion using *Pou2f3-Cre-Ert2* led to the same clearance delay 7 dpi (Fig.
638 5J). Worm burdens were equivalent in CRE-positive and -negative mice 5 dpi,
639 suggesting normal colonization of the SI by *Nb* arriving from the lung. The delayed
640 clearance was also not due to the loss of one *Pou2f3* allele in *Chat*$^{fl/fl}$*;Pou2f3*$^{Cre\text{-}ERT2/+}$
641 mice as they cleared worms normally when not treated with tamoxifen (Fig. S5R). In
642 order allow initiation of type 2 remodeling to proceed normally and delete tuft cell ACh
643 only during worm clearance, we waited until 5 dpi to administer a single dose of
644 tamoxifen to *Chat*$^{fl/fl}$*;Vil1-Cre-ERT2* mice. Consistent with our earlier observation that
645 tamoxifen suppresses intestinal Type 2 immunity, worm clearance in WT mice was
646 delayed to day 8, but we again found a *Chat*-dependent delay in worm clearance
647 despite normal intestinal remodeling. (Fig. 5K, Fig. S5S-T). Thus, we propose that tuft-
648 cell derived ACh contributes to worm clearance by the induction of epithelial fluid
649 secretion.
650

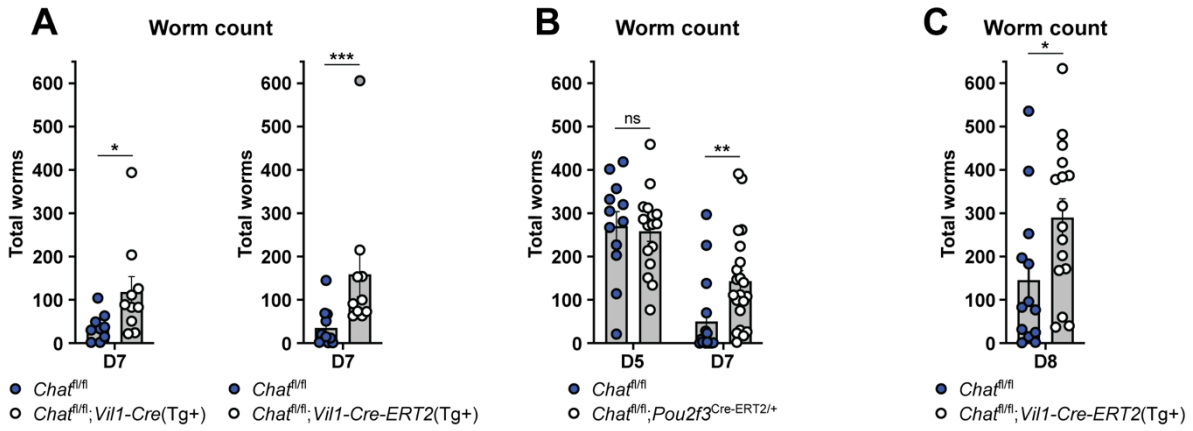

Figure 6: Tuft cell-derived ACh contributes to helminth clearance. (**A** and **B**) Quantification of total SI *Nb* in mice of indicated genotypes at (A) 7 or (B) indicated days post infection. (**C**) Quantification of total SI *Nb* 8 days post infection in mice of indicated genotypes given single dose of tamoxifen on D5. In the graphs, each symbol represents an individual mouse pooled from two or more experiments. *p < 0.05, **p < 0.01, ***p < 0.001, ****p < 0.001 by Mann-Whitney test (A, C), or multiple Mann-Whitney tests with Holm Sídák's multiple comparisons test (B). ns, not significant. Graphs depict mean +/- SEM. Also see Fig. S6.

Discussion

This study identifies an epithelium-intrinsic response unit that couples tuft cell chemosensing to epithelial fluid secretion via the release of ACh from tuft cells. This effector function is common to tuft cells in multiple tissues and is executed within seconds of activation. In the SI, tuft cell-derived ACh is required for timely clearance of helminth infection, but unlike all previously identified tuft cell effector functions, tuft cell-derived ACh does not impact ILC2 activation nor downstream intestinal remodeling. Instead, it appears that tuft cell ACh provides an acute signal that contributes to the weep and sweep responses that push worms out of the intestine. The magnitude of tuft cell-dependent fluid secretion correlates with the number of *Chat*+ tuft cells, suggesting one possible function for the tuft cell hyperplasia that occurs even after initial sensing of the helminth has been achieved.

Some details of tuft cell-regulated fluid secretion remain unresolved. For example, we do not understand the regulation of *Chat* in SI tuft cells. It is unclear why only a subset of SI tuft cells are *Chat*+, why there is a proximal to distal gradient of *Chat*+ tuft cells, and why the frequency of *Chat*+ tuft cells decreases during Type 2

676 inflammation (although the total number increases due to tuft cell hyperplasia).
677 Furthermore, most tuft cells do not express *Slc5a7*, which encodes CHT1, the
678 transporter that neurons use to import choline for ACh synthesis, nor *Slc18a3*, which
679 encodes VAChT, a transporter that loads ACh into secretory vesicles in neurons.[70]
680 Lastly, it remains to be seen whether tuft cell-derived ACh also induces bicarbonate
681 secretion, as this often occurs together with chloride release and further supports the
682 unfolding of extracellular mucus.[71]
683 We have also not identified the precise ACh receptor(s) that mediate(s) the fluid
684 secretion response, although inhibition by atropine implicates a muscarinic rather than
685 nicotinic receptor. are the only detectable muscarinic receptor transcripts in
686 unmanipulated SI epithelium[9,11] and *Nb* clearance is delayed in *Chrm3*$^{-/-}$ mice.[40]
687 Induction of Type 2 cytokines is also impaired in these *Chrm3*$^{-/-}$ mice, so conditional
688 *Chrm* alleles will be needed to identify in which cells the receptors are required and for
689 which aspects of Type 2 immunity.
690 While tuft cell-derived ACh was not required for ILC2 activation during helminth
691 infection and intestinal remodeling was largely intact, there were slight yet significant
692 defects in tuft cell numbers or SI length at some timepoints analyzed. Prior literature has
693 shown that deletion of *Chrm3* from the SI epithelium causes an *increase* in tuft cell
694 numbers at baseline but a *decrease* in tuft cells following irradiation.[67] Perhaps epithelial
695 ACh signaling has damaged-induced functions that overlap with helminth-induced
696 intestinal remodeling. Regulation of intestinal epithelial differentiation by tuft cell-derived
697 ACh bears further study.
698 We have focused on tuft cell ACh signaling on enterocytes to drive fluid
699 secretion, but ACh receptors are expressed by many cells, including other types of
700 intestinal epithelial cells. Goblet cells undergo compound exocytosis of mucus in
701 response to ACh,[46,47,72] and the formation of goblet-associated antigen passages
702 (GAPs) has also been linked to ACh signaling.[73,74] Additionally, tuft cell ACh was
703 recently reported to induce mucus secretion from cholangiocytes in the gallbladder.[57]
704 We therefore extensively tested the hypothesis that ACh from SI tuft cells signals on
705 villus goblet cells to induce mucus secretion and GAP formation, but we could not find
706 any evidence that this occurs *in vivo* (data not shown). A recent study demonstrating

707 that muscarinic receptor expression is restricted to GCs at the base of SI crypts, and
708 that only these cells respond acutely to CCh,[75] may explain why we did not detect tuft
709 cell-dependent regulation of GC mucus secretion. While it remains possible that ACh
710 from SI crypt tuft cells regulates secretion by GCs (and Paneth cells), we generally
711 found fewer *Chat*+ tuft cells in the crypts than in the villi, and chemosensing pathways
712 are likely not yet functional in immature crypt tuft cells. Perhaps in the colon tuft cell
713 ACh regulates the function of sentinel GCs at crypt openings.[76] Lastly, ACh-regulated
714 smooth muscle contraction is critical for SI helminth clearance[28,37] and tuft cells have
715 been linked to smooth muscle function in other tissues.[19,57] The short extracellular half-
716 life of ACh combined with the distance between epithelial tuft cells and smooth muscles
717 that surround the SI make direct signaling unlikely. Nonetheless, while we did not see
718 evidence of direct contact between tuft cells and enteric neurons, they have been
719 previously reported in the SI[10,77,78] and thus we cannot rule out the possibility that tuft
720 cell ACh regulates smooth muscle contraction via the enteric nervous system.
721 During Type 2 inflammation in the SI, the maximal fluid secretion induced by ACh
722 is dramatically reduced,[69] possibly to prevent excessive fluid loss or diarrhea during
723 chronic helminth infection. At the same time, the number of *Chat*+ tuft cells increases,
724 such that tuft cell-regulated fluid secretion is maintained or even enhanced compared to
725 baseline. This re-wiring of ACh-regulated fluid secretion may represent a regulatory
726 mechanism that minimizes fluid loss due to endogenous signals while maintaining the
727 ability to respond to lumen-restricted agonists such as helminths via tuft cell sensing. In
728 that regard, tuft cells also have an advantage over mast cells and neurons, which can
729 induce enhanced fluid secretion during Type 2 inflammation via release of histamine
730 and/or prostaglandin E2,[69] but can only respond to ligands that penetrate the mucosal
731 barrier. Relatedly, it remains unclear whether the acetylcholinesterases secreted by
732 helminths can penetrate the mucosal barrier to target ACh in the tissue, or whether
733 helminths are only able to counter the effects of ACh during tissue-dwelling phases of
734 their lifecycle.
735 Although we have focused on the SI in this study, we propose tuft cells link
736 chemosensing to fluid secretion in all tissues. Indeed, with the exception of tuft-ILC2
737 circuit activation, all other known tuft cell effector functions occur instantaneously and

738 seem to mediate evasion (e.g. breathing cessation)[14,16] and expulsion (e.g. mucociliary
739 sweep) of microbes and other agonists.[8,17] Fluid secretion fits this paradigm. The
740 mucosal barrier must be constantly hydrated and fluid secretion can provide a flushing
741 effect. Based on the ligands tuft cells sense in different tissues, such mechanisms could
742 be important to clear allergens from the upper airways or bacteria from the trachea and
743 urethra. Tuft cell sensing may also reduce baseline fluid secretion, as one recent study
744 suggested.[79] The ligands and function of tuft cells in the colon are only just being
745 elucidated,[56] but we predict that tuft cell-regulated fluid secretion would help maintain a
746 healthy mucosal barrier here too. Tuft cell frequency is generally decreased in patients
747 with active inflammatory bowel disease,[80,81] consistent with a role for tuft cells in
748 preventing bacterial infiltration. Conversely, increased tuft cell frequency was detected
749 in colonic biopsies from patients with diarrhea-predominant irritable bowel syndrome, a
750 largely non-inflammatory condition of unknown origin.[82]
751 Why tuft cells sense succinate in either the SI or, as we have now demonstrated,
752 the trachea, remains unclear. We could not find any impact of tuft cell *Chat* deletion on
753 *Tritrichomonas* burden or distribution, but perhaps tuft cell-mediated fluid secretion,
754 together with IL-13-induced anti-microbial peptides and mucus production, acts more
755 locally to keep microbes away from the epithelium.[83] Succinate levels have also been
756 shown to increase in contexts of bacterial dysbiosis, and inducing tuft cell hyperplasia
757 with succinate treatment reduces inflammation in a model of ileitis.[80] As for the trachea,
758 aberrant release of cellular succinate into the airways, which occurs in some patients
759 with cystic fibrosis, can promote colonization and biofilm formation by the
760 pathosymbiont *Pseudomonas aeruginosa.*[84] Induction of CFTR-dependent fluid
761 secretion by prostaglandin E2 released from airway tuft cells has also been
762 suggested.[86] Thus, tracheal tuft cells may induce fluid secretion to flush away succinate
763 and other soluble molecules and to deter bacterial accumulation.
764 Therapeutically, benefit may be achieved by tuning tuft cell effector functions up
765 or down, depending on the context and need. For example, tuft cell-induced fluid
766 secretion may prove useful in treating cystic fibrosis patients in whom CFTR-dependent
767 fluid secretion is impaired, while certain patients suffering from diarrhea might benefit

768 from reduced tuft cell function. Future study should investigate the involvement of tuft
769 cell-induced fluid secretion in human disease.
770

771 **Acknowledgements:**

772 We thank all members of the von Moltke lab for helpful discussion and input on this
773 manuscript. We thank D. Hailey and the Garvey Cell Imaging Lab in the Institute for
774 Stem Cell & Regenerative Medicine for microscopy support; the mouse husbandry staff
775 in the UW SLU vivarium; V. Gersuk, K. O'Brien and the Benaroya Research Institute
776 Genomics Core for help with RNA sequencing; and M. F. Fontana for helpful comments
777 on the manuscript. Flow cytometry data were acquired through the University of
778 Washington, Cell Analysis Facility Shared Resource Lab, with NIH award
779 1S10OD024979-01A1 funding for the Symphony A3. We thank Takeda for the generous
780 gift of the Class 8 TRPM5 agonist.

781 **Funding**

782 TEB was supported by the UW Immunology Fellowship, and DLJ was a UW Mary Gates
783 scholar. MMM is a Hannah H. Gray fellow and JvM is a Searle Scholar and a Burroughs
784 Wellcome Investigator in the Pathogenesis of Infectious Disease. Work at the University
785 of Washington was supported by NIH DP2OD024087, R01AI145848, and
786 R01AI167923. Work at Stanford was supported by NIH R01DK128292 and
787 R21AI171222 (MRH). CF is an A.P. Giannini Fellow and was also supported by the
788 Stanford School of Medicine Dean's Postdoctoral Fellowship and Stanford Maternal &
789 Child Health Research Institute Postdoctoral Fellowship. Work at Seattle Children's
790 Research Institute was supported by NIH R01HL128361 (JSD) and K24AI150991
791 (JSD).

792 **Contributions:**

793 TEB designed and performed experiments, analyzed data, and wrote the paper with
794 JVM. LMW, DBS, MMM, DNK, and JWM assisted with experiments at the University of
795 Washington. CF and MBG performed *in vivo* Class 8 and *T. musculis* fecal water

content experiments at Stanford University with supervision and funding provided by MRH. KAB and LMR performed pilot Ussing chamber experiments with supervision and funding provided by JSD. AB, MS, and RM led the development and validation of the Class 8 TRPM5 agonist at Takeda Pharmaceuticals in collaboration with Evotec. JVM conceived of and supervised the study, analyzed data, acquired funding, and wrote the paper with TEB.

Methods:

Study Design

All experiments were performed using randomly assigned mice without investigator blinding. No data were excluded, except from Ussing chambers when mounted tissues failed to respond to stimulation by a positive control (e.g. CCh). All data points reflect biological replicates, except for *in vitro* ILC2 stimulations and epithelial monolayer experiments where each data point is a technical replicate. Data were pooled from multiple experiments unless otherwise noted. The number of independent experiments is included in the figure legends.

Experimental Animals

Mice aged 6 weeks and older were used for all experiments. Mice were age-matched within each experiment. Pooled results include both male and female mice of varying ages unless otherwise indicated. Mouse strains used in this study are listed in Table S3. Acute deletion of conditional alleles in mice was achieved by oral gavage with tamoxifen dissolved in corn oil (100 mg/kg). *Chat*$^{fl/fl}$*;Vil1-Cre-ERT2(Tg+)* mice were administered tamoxifen on day -4 and 0 of infection with *N. brasiliensis* and on day -6 and -4 of treatment with 150 mM succinate drinking water, or as noted in the text. *Chat*$^{fl/fl}$*;Pou2f3*$^{Cre\text{-}ERT2/+}$ mice were administered tamoxifen every other day starting on day -4 of *N. brasiliensis* infection or as noted in the text. *DREADD(Tg+); Pou2f3*$^{Cre\text{-}ERT2/+}$ mice were administered tamoxifen chow for 7 days prior to Ussing experiments. All mice (CRE+ and CRE-) received tamoxifen treatment. All mice were maintained in specific pathogen-free conditions at the University of Washington or Stanford University and were confirmed to be free of *Tritrichomonas sp.* by microscopy and qPCR, unless

826 specifically colonized for experimental purposes. All procedures were conducted within
827 University of Washington or Stanford University (Class 8 gavage) IACUC guidelines
828 under approved protocols.
829
830 **Measuring epithelial ion flux with Ussing chambers**
831 All Ussing chamber protocols were modified from Clarke et al.[51]
832
833 *Tissue mounting*: Mice 7-12 weeks of age were euthanized by CO_2 and segments of the
834 intestine (SI, cecum, colon) were harvested and flushed with cold Krebs Buffered
835 Ringer's solution + mannitol (10 mM D-mannitol, 115 mM NaCl, 2.4 mM K_2HPO_4, 0.4
836 mM KH_2PO_4, 25 mM $NaHCO_3$, 1.2 mM $CaCl_2$ dihydrate, 1.2 $MgCl_2$ hexahydrate; pH
837 7.25-7.4). Intestines (first 5 cm of pSI and last 5 cm of dSI) were fileted open along the
838 mesenteric line, trimmed and mounted to the pins of an Ussing chamber cassette with
839 aperture of 0.3 cm^2 (Physiologic Instruments, Reno, USA), avoiding Peyer's patches.
840 For some experiments the SI was pinned to a Sylgard-coated plate with the serosal side
841 up and the muscle layer scored with a scalpel and "stripped" away using forceps under
842 a dissection scope. The resulting epithelium-submucosa tissue was mounted in a
843 cassette as normal. For trachea preparations, the entire trachea was harvested,
844 surrounding tissue (esophagus) removed, and cut open lengthwise along the anterior
845 side (away from esophagus) for mounting in a 2 mm^2 aperture cassette (Physiologic
846 Instruments, Reno, USA). Cassettes containing tissues were mounted in Ussing
847 chambers (Physiologic Instruments, Reno, USA) and the lumenal chambers filled with 5
848 mL of KBR + mannitol and the basolateral chambers filled with 5 mL of KBR + glucose
849 (10 mM D-glucose, 115 mM NaCl, 2.4 mM K_2HPO_4, 0.4 mM KH_2PO_4, 25 mM $NaHCO_3$,
850 1.2 mM $CaCl_2$ dihydrate, 1.2 $MgCl_2$ hexahydrate; pH 7.25-7.4). The chambers were
851 warmed to 37C and bubbled with carbogen (95% O_2, 5% CO_2) for the duration of the
852 experiment. For Cl^- replacement experiments, Cl^- free KBR was used, in which
853 gluconate is substituted for Cl- (115 mM D-gluconic acid sodium salt, 2.4 mM K_2HPO_4,
854 0.4 mM KH_2PO_4, 25 mM $NaHCO_3$, 4 mM calcium D-gluconate monohydrate, 1.2 mM
855 magnesium D-gluconate hydrate; pH 7.25-7.4).
856

857 *Measuring the short circuit current (Isc)*: Automatic voltage clamping was performed by
858 MultiChannel Voltage-Current Clamp (Physiologic Instruments, Reno, USA). Voltage
859 differences between electrodes and fluid resistance of the buffer were compensated
860 prior to insertion of the tissue cassette. Isc was measured by voltage clamp every 1
861 second and recorded using Acquire & Analyze software (Physiologic Instruments, Reno,
862 USA) and normalized to tissue area. After a 20 min equilibration period, tissues were
863 stimulated lumenally with Na_2-succinate (1, 10 mM) or cis-epoxysuccinic acid (10 mM),
864 basolaterally with 5 μM Class 8, or bilaterally with 1 μM Compound 21. For
865 succinate/cESA stimulation, subsequent stimulations were administered every 10 min;
866 for Class 8 the interval was increased to 15 min due to the slower kinetics of the
867 response. Subsequent stimulations included lumenal 20 mM NaCl, basolateral 100 uM
868 CCh, and bilateral cocktail of 100 uM 3-Isobutyl-1-methylxanthine (IBMX) + 10 uM
869 forskolin. Chemical inhibitors were administered 5 min after start of equilibration period
870 (15 min before first stimulation): basolateral 100 μM bumetanide, bilateral 10 μM
871 ibuprofen, basolateral 10 μM atropine, basolateral 1 μM tetrodotoxin, and lumenal 1 mM
872 carbenoxolone. ΔIsc values were calculated as the difference between the Isc
873 measurement at the peak of the stim response and the Isc measurement taken right
874 before adding the agonist. For tissues that did not respond to the agonist (e.g., knockout
875 mouse intestines, tissues treated with inhibitors) and therefore had no peak response,
876 the Isc value was taken at the same timepoint as the peak Isc value for the
877 corresponding WT or control tissue.
878
879 **Measuring fecal water content**
880 Mice were orally gavaged with vehicle (0.5% methylcellulose + 1% Tween 20) or 30
881 mg/kg Class 8, and fecal samples (2+ pellets) were taken at 0 and 3 hours post gavage.
882 For protist-colonized experiments, B6 mice were colonized with *T. musculis* protists and
883 fecal samples collected at 2, 7,14, and 20 days post colonization. Fecal samples were
884 dried at 60C overnight and % water content calculated as (1-(dry weight/wet
885 weight))*100.
886
887 **Monolayer culture and cysteinyl leukotriene ELISA**

888 Proximal small intestine was isolated and villi were gently scraped off with a glass
889 coverslip. Tissue was incubated for 30 minutes at 4° with 2mM EDTA to release
890 epithelial crypts, then washed twice with cold PBS and filtered through a 70um strainer.
891 Crypts were resuspended in complete monolayer media (DMEM/F12 supplemented
892 with 2mM glutamine, 100U/mL penicillin, 100mg/mL streptomycin, 10mM HEPES, N2
893 supplement, B27 supplement, R-spondin (10% supernatants from R-spondin secreting
894 cells), Noggin (10% supernatant from Noggin secreting cells), 500mM N-acetylcysteine,
895 50ug/mL mEGF, and 10uM Y27632). Plates were coated with 2% Matrigel in cold
896 DMEM/F12 and incubated at 37° for at least 30 minutes. Media was aspirated from the
897 plate, and 1000 crypts were plated per well of a 48-well plate. Crypts were incubated
898 overnight, and non-adherent cells were aspirated the next day. Test stimuli diluted in
899 HBSS containing Ca2+/Mg2+ were added to monolayers and stimulated at 37° for 30
900 minutes. Supernatants were collected and used for the Cysteinyl Leukotriene Express
901 ELISA kit (Cayman Chemical) according to manufacturer's protocol.
902
903 **Succinate and cytokine treatment**
904 For succinate experiments mice were given 150mM sodium succinate hexahydrate
905 (Thermo) ad libitum in drinking water for the indicated amount of time. Recombinant
906 murine IL-25 (500 ng; R&D) was given for 3 consecutive days intraperitoneally in 200 µL
907 PBS.
908
909 **Helminth infections and analysis**
910 *N. brasiliensis* larvae were raised and maintained as previously described.[85]
911 Mice were infected subcutaneously with 500 *N. brasiliensis* L3. At sacrifice, the entire SI
912 was fileted open and total worms counted under a stereomicroscope.
913
914 **Protist colonization and analysis**
915 Breeding pairs were colonized with *Tritrichomonas musculis* or *T. rainier* as previously
916 described.[87] Pups from colonized breeding pairs were analyzed. Protist numbers were
917 quantified by flow cytometry as described by Chudnovskiy et al.[88] Briefly, 10 cm of pSI
918 and dSI were flushed into a 15 mL conical with 10 mL RT PBS using a gavage needle.

919 Cecal contents were harvested into 15 mL conical, weighed, and then 10 mL RT PBS
920 added. Samples were let sit for 30 min at RT, vortexed, and then passed through a 70
921 µm filter. Protists were washed, stained with DAPI, then count beads added and data
922 collected on a FACSCanto II (BD Biosciences). Protist numbers per gram of cecal
923 content was calculated.
924
925 **Intestinal tissue fixation and staining**
926 Intestinal tissues were flushed with PBS and fixed in 4% paraformaldehyde for 3-4
927 hours at 4°C, washed with PBS, and incubated in 30% (w/v) sucrose overnight at 4°C.
928 Samples were then coiled into "Swiss rolls", embedded in Optimal Cutting Temperature
929 Compound (Tissue-Tek) and sectioned at 8 µm on a CM1950 cryostat (Leica).
930 Immunofluorescent staining was performed in PBS with 1% BSA at room temperature
931 as follows: 1 hr 10% donkey serum with 1:1000 Fc Block, 1 hr (or O/N at 4°C) primary
932 antibody, 5 min wash, 45 min secondary donkey antibody and/or WGA-488, 5 min
933 wash, and mounted with Vectashield plus DAPI (Vector Laboratories). Images were
934 acquired with an Axio Observer A1 (Zeiss) microscope with a 10X or 20X A Plan
935 objective. Tuft cell frequency was calculated using ImageJ software to manually quantify
936 DCLK1^{+} cells per millimeter of crypt-villus axis. Goblet cell frequency was calculated
937 using ImageJ software to manually quantify total WGA+ cells in the villus (crypts were
938 excluded because WGA also labels Paneth cells) per millimeter of crypt villus axis. For
939 each replicate, four 10x images of the Swiss roll were analyzed and at least 25 total villi
940 counted.
941
942 **Single-cell tissue preparation for flow cytometry**
943 For single cell epithelial preparations from SI, tissues were flushed with PBS,
944 Peyer's patches removed, opened longitudinally, and rinsed with PBS. Tissue was cut
945 into small pieces, shaken vigorously for 20 seconds in 30 mL cold HBSS (Ca^{+2}/Mg^{+2}-
946 free) with 1 mM HEPES, drained, and then incubated rocking at 37°C for 10 min in 15
947 mL HBSS (Ca^{+2}/Mg^{+2}-free) supplemented with 3 mM EDTA and 1 mM HEPES. Tissues
948 were vortexed thoroughly and released epithelial cells passed through a 70 µm filter.
949 This process was repeated for a total of 3 rounds. Supernatants were pooled and

950 washed with HBSS (Ca^{+2}/Mg^{+2}-free) with 1 mM HEPES before staining for flow
951 cytometry.
952 For lamina propria (LP) preparations from uninfected mice, SI was processed as
953 above to remove the epithelial fraction. Tissues were then incubated shaking at 37°C for
954 30 minutes in 10 mL RPMI 1640 supplemented with 20% FCS, 1 mM HEPES, 0.05
955 mg/ml DNase I (Sigma Aldrich), and 1 mg/mL Collagenase A (Sigma Aldrich). Tissues
956 were vortexed and cells were passed through a 100 μm filter, then a 40 μm filter,
957 washing with cold HBSS (Ca^{+2}/Mg^{+2}-free) with 1 mM HEPES. Cells were washed and
958 stained for flow cytometry.
959 For LP preparations from *N. brasiliensis*-infected mice (D4), mice were
960 anaesthetized with 5% avertin. The peritoneal cavity was opened, the SI nicked at the
961 junction with the stomach and transected at the cecum and flushed with 20 mL of 37°C
962 HBSS (Ca^{+2}/Mg^{+2}-free) plus 1 mM HEPES. Then the mice were perfused through the
963 heart with 30 mL of 37°C HBSS (Ca^{+2}/Mg^{+2}-free) with 30 mM EDTA and 1 mM HEPES.
964 Three minutes after perfusion was completed, the first 10 cm of the proximal SI was
965 harvested, Peyer's patches removed, opened longitudinally, and cut into small pieces
966 and shaken vigorously for 20 seconds in 30 mL cold HBSS (Ca^{+2}/Mg^{+2}-free) with 1 mM
967 HEPES, then drained. Tissues were then digested and processed as above in
968 uninfected mice.
969 For mesenteric lymph node (MLN) preparations, SI-draining MLN were harvested
970 into RPMI + 5% FBS on ice, mashed through a 70 μm filter, the filter washed with RPMI
971 + 5% FBS, and cells washed and stained for flow cytometry.
972
973 **Flow cytometry and cell sorting**
974 Single cell suspensions from tissues were prepared as described above. For flow
975 cytometry, SI epithelium and MLN samples were stained in DPBS (Ca^{+2}/Mg^{+2}-free) with
976 3% FCS and LP samples were stained in PBS (Ca^{+2}/Mg^{+2}-free) with 3% FCS, 2 mM
977 EDTA, and 0.02 mg/mL DNase I with antibodies to surface markers for 30 min at 4°C,
978 followed by DAPI (Roche) for dead cell exclusion. When cell counts were needed,
979 counting beads (Spherotech) were added prior to running flow cytometry. Samples were
980 run on a FACSCanto II or LSRII (BD Biosciences) and analyzed with FlowJo 10.8.1.

981 Samples were FSC-A/SSC-A gated to exclude debris, FSC-A/FSC-H gated to select
982 single cells, and gated to exclude dead cells. For cell sorting, single cell suspensions
983 were prepared and stained as described and sorted on an Aria III (BD Biosciences).
984
985 **ILC2 Stimulation Assay**
986 Entire SILP from several mice were pooled and ILC2s (EpCAM-, CD45^{+}, Lin(CD3, CD4,
987 CD5, CD8, CD11b, CD19, NK1.1, FcER1)$^{-}$, KLRG1^{+}) sorted as described. Sorted cells
988 were plated at 5000 cells per well in a 96-well plate and incubated at 37°C overnight in
989 10 ng/ml IL-7 (R&D Systems) and basal media composed of high glucose DMEM
990 supplemented with non-essential amino acids, 10% FBS, 100 U/mL penicillin,
991 100mg/mL streptomycin, 10mM HEPES, 1mM sodium pyruvate, 100μM 2-
992 mercaptoethanol, and 2mM L-glutamine. The next morning, media was replaced and
993 cells were stimulated with the indicated agonist. After a six-hour stimulation,
994 supernatant was collected and the cells were washed and stained with 1 uL/well of PE-
995 conjugated anti-human CD4 for 20 min at 4°C. Cells were washed, resuspended in
996 DAPI and analyzed on a CantoRUO (BD Biosciences). Cytokine levels in supernatants
997 were measured using Enhanced Sensitivity Flex Sets (BD Biosciences) for mouse IL-5
998 and IL-13 according to the manufacturer's protocol. Data was collected on an LSRII (BD
999 Biosciences).
1000
1001 **RNA Sequencing and Analysis**
1002 150-200 tuft cells were sorted directly into lysis buffer from the SMART-Seq v4 Ultra
1003 Low Input RNA Kit (Takara) and cDNA generated following manufacturer's instructions.
1004 Cells were sorted from four individual mice for each experiment. Sequencing libraries
1005 were generated using the Nextera XT library preparation kit with multiplexing primers,
1006 according to manufacturer's protocol (Illumina), and library quality assessed using
1007 Tapestation (Agilent). High throughput sequencing was performed on NextSeq 2000
1008 (Illumina), sequencing dual-indexed and paired-end 59 base pair reads. All samples
1009 were in the same run with a target depth of 5 million reads. Base calls were processed
1010 to FASTQs on BaseSpace (Illumina), and a base call quality-trimming step was applied
1011 to remove low-confidence base calls from the ends of reads. The FASTQs were aligned

1012 to the GRCm38 mouse reference genome, using STAR v.2.4.2a and gene counts were
1013 generated using htseq-count. Further analysis of the data was performed using the
1014 DIY.Transcriptomics (diytranscriptomics.com) pipeline, with experiment-specific
1015 modifications. Samples were filtered to exclude genes with counts per million = 0 in 4 or
1016 more samples and genes annotated as pseudogenes. Finally, samples were normalized
1017 to each other. To identify differentially expressed genes, precision weights were first
1018 applied to each gene based on its mean-variance relationship using VOOM,[89] then data
1019 was normalized using the TMM method[90] in EdgeR.[91] Linear modeling and bayesian
1020 stats were employed via Limma[92] to find genes that were up- or down-regulated by 2-
1021 fold (Log2FC = 1) or more, with a false-discovery rate (FDR) of 0.01. The code and
1022 results for these analyses are included as Data File S1 and S2.
1023
1024 **Statistical Analysis**
1025 Statistical analysis was performed as noted in figure legends using Prism 9 (GraphPad)
1026 software. Graphs show mean +/- SEM.
1027

1028 **Table S3**

Reagent or Resource	Source	Identifier
B6.Cg-Tg(RP23-268L19-EGFP)2Mik/J (Chat-GFP)	Jackson Laboratory	JAX #007902
B6.*Il25*$^{Flare25/Flare25}$ (Il25-RFP)	R. Locksley (PMID: 26675736)	NA
B6.*Il13*$^{Smart13/Smart13}$ (Smart13)	R. Locksley (PMID: 22138715)	NA
C57BL/6N-Pou2f3<tm1(KOMP)Vlcg>/Tcp (*Pou2f3*$^{-/-}$)	Canadian Mouse Mutant Repository	CMMR #ABDF
B6.129P2-Trpm5^{tm1Dgen}/J (Trpm5$^{-/-}$)	Jackson Laboratory	JAX #005848
B6.*Sucnr1*$^{-/-}$	In-house (PMID: 30021144)	NA
B6.*Il25*$^{-/-}$	A. McKenzie (PMID: 16606668)	NA
B6;129-Chat^{tm1Jrs}/J (*Chat*$^{fl/fl}$)	Jackson Laboratory	JAX #016920
B6.Cg-Tg(Vil1-cre)997Gum/J	Jackson Laboratory	JAX #004586
B6.Cg-Tg(Vil1-cre)1000Gum/J (Vil1-Cre1000)	Jackson Laboratory	JAX #021504
B6.Cg-Tg(Vil1-cre/ERT2)23Syr/J (*Vil1-Cre-Ert2*)	Jackson Laboratory	JAX #020282
B6(129S4)-*Pou2f3*$^{tm1.1(cre/ERT2)Imt}$/J (Pou2f3-Cre-Ert2)	Jackson Laboratory	JAX #037511
B6.129S-Chattm1(cre)Lowl/MwarJ (*Chat-Cre*)	Jackson Laboratory	JAX #031661
B6.*Il25-Cre*	R. Locksley (PMID: 35245089)	NA
B6.Cg-*Gt(ROSA)26Sor*$^{tm9(CAG-tdTomato)Hze}$/J (Ai9)	Jackson Laboratory	JAX #007909
B6N;129-Tg(CAG-CHRM3*,-mCitrine)1Ute/J (Gq-DREADD)	Jackson Laboratory	JAX #026220
B6.129-*Gt(ROSA)26Sor*$^{tm1(CAG-CHRM4*,-mCitrine)Ute}$/J (Gi-DREADD)	Jackson Laboratory	JAX #026219
B6.*Alox5*$^{fl/fl}$	In-house (PMID: 32160525)	NA
B6.*Il4ra*$^{fl/fl}$	F. Brombacher (PMID: 15142530)	NA

1029

1030 **Table S4**

Reagent or Resource	Dilution Factor	Source	Identifier
Rabbit α-DCLK1	1:1000	Abcam	Cat#ab31704
Rabbit α-TUJ1 (Beta-III tubulin)	1:500	Abcam	Cat#ab18207
Goat α-GFP	1:500	Novus Bio	Cat#NB100-1770
Rabbit α-dsRed	1:500	Clontech	Cat#632496
Rabbit α-HA, clone 16B12	1:1000	Biolegend	Cat#901516
WGA-488	1:150	Thermo	Cat#W11261
Donkey α-Rabbit IgG AF594	1:1000	Thermo	Cat#A-21207
Donkey α-Goat IgG AF488	1:500	Thermo	Cat#A-11055
CD16 / CD32, clone 2.4G2	1:1000	Tonbo	Cat# 70-0161-M001
CD3 PerCP-Cy5.5, clone 145-2C11	1:100	Biolegend	Cat#100328
CD3 BV421, clone 145-2C11	1:400	Biolegend	Cat#100335
CD4 BV711, clone RM4-5	1:250	Biolegend	Cat#100549
CD4 eF450, clone RM4-5	1:200	eBioscience	Cat# 48-0042-80
hCD4 PE, clone RPA-T4	1:50	Biolegend	Cat#300508
CD5 PerCP-Cy5.5, clone 53-7.3	1:500	Biolegend	Cat#100624
CD5 eF450, clone 53-7.3	1:400	Biolegend	Cat#100607
CD8 PerCP-Cy5.5, clone 53-6.7	1:200	Biolegend	Cat#100724
CD8 BV421, clone 53-6.7	1:400	Biolegend	Cat#100737
CD11b AF700, clone M1/70	1:250	Biolegend	Cat#101222
CD11b BV421, clone M1/70	1:400	Biolegend	Cat# 101235
CD19 PerCP-Cy5.5, clone 6D5	1:250	Biolegend	Cat#115533
CD19 BV421, clone 6D5	1:400	Biolegend	Cat# 115537

CD24 PE, clone M1/69	1:300	Biolegend	Cat#101807
CD24 PerCP-Cy5.5, clone M1/69	1:300	Biolegend	Cat#101824
CD45 BV605, clone 30F11	1:300	Biolegend	Cat#103155
CD45 BV650, clone 30F11	1:500	Biolegend	Cat#103151
EpCAM PE-Dazzle, clone G8.8	1:300	Biolegend	Cat#118235
EpCAM AF488, clone G8.8	1:300	Biolegend	Cat#118210
EpCAM PE-Cy7, clone G8.8	1:300	Biolegend	Cat#118215
FcER1 BV421, clone Mar-1	1:400	Biolegend	Cat#334623
IL17RB APC, clone 9B10	1:100	Biolegend	Cat#146307
KLRG1 PE-Cy7, clone 2F1	1:250	Biolegend	Cat#138416
NK1.1 PerCP-Cy5.5, clone PK136	1:100	Biolegend	Cat#108728
NK1.1 BV421, clone PK136	1:200	Biolegend	Cat#108731
Siglec-F APC-Cy7, clone E50-2440	1:100	BD	Cat#565527
Siglec-F AF647, clone E50-2440	1:100	BD	Cat# 562680
Thy1.2 (CD90.2) BV605, clone 53-2.1	1:500	Biolegend	Cat#140318

1031
1032
1033
1034
1035

1036 **References**

1037 1. Frizzell, R.A., and Hanrahan, J.W. (2012). Physiology of epithelial chloride and fluid
1038 secretion. Cold Spring Harb Perspect Med *2*, a009563.
1039 10.1101/cshperspect.a009563.

1040 2. Cooke, H.J. (1998). “Enteric Tears”: Chloride Secretion and Its Neural Regulation.
1041 News Physiol Sci *13*, 269–274.

1042 3. Xue, J., Askwith, C., Javed, N.H., and Cooke, H.J. (2007). Autonomic nervous system
1043 and secretion across the intestinal mucosal surface. Auton Neurosci *133*, 55–63.
1044 10.1016/j.autneu.2007.02.001.

1045 4. Hirota, C.L., and McKay, D.M. (2006). Cholinergic regulation of epithelial ion transport
1046 in the mammalian intestine. Br J Pharmacol *149*, 463–479. 10.1038/sj.bjp.0706889.

1047 5. Cox, M.A., Bassi, C., Saunders, M.E., Nechanitzky, R., Morgado-Palacin, I., Zheng,
1048 C., and Mak, T.W. (2020). Beyond neurotransmission: acetylcholine in immunity and
1049 inflammation. J Intern Med *287*, 120–133. 10.1111/joim.13006.

1050 6. Mashimo, M., Moriwaki, Y., Misawa, H., Kawashima, K., and Fujii, T. (2021).
1051 Regulation of Immune Functions by Non-Neuronal Acetylcholine (ACh) via
1052 Muscarinic and Nicotinic ACh Receptors. Int J Mol Sci *22*, 6818.
1053 10.3390/ijms22136818.

1054 7. Yajima, T., Inoue, R., Matsumoto, M., and Yajima, M. (2011). Non-neuronal release
1055 of ACh plays a key role in secretory response to luminal propionate in rat colon. J
1056 Physiol *589*, 953–962. 10.1113/jphysiol.2010.199976.

1057 8. Perniss, A., Liu, S., Boonen, B., Keshavarz, M., Ruppert, A.-L., Timm, T., Pfeil, U.,
1058 Soultanova, A., Kusumakshi, S., Delventhal, L., et al. (2020). Chemosensory Cell-
1059 Derived Acetylcholine Drives Tracheal Mucociliary Clearance in Response to
1060 Virulence-Associated Formyl Peptides. Immunity *52*, 683-699.e11.
1061 10.1016/j.immuni.2020.03.005.

1062 9. Haber, A.L., Biton, M., Rogel, N., Herbst, R.H., Shekhar, K., Smillie, C., Burgin, G.,
1063 Delorey, T.M., Howitt, M.R., Katz, Y., et al. (2017). A single-cell survey of the small
1064 intestinal epithelium. Nature *551*, 333–339. 10.1038/nature24489.

1065 10. Bezençon, C., Fürholz, A., Raymond, F., Mansourian, R., Métairon, S., Le
1066 Coutre, J., and Damak, S. (2008). Murine intestinal cells expressing Trpm5 are
1067 mostly brush cells and express markers of neuronal and inflammatory cells. J Comp
1068 Neurol *509*, 514–525. 10.1002/cne.21768.

1069 11. Nadjsombati, M.S., McGinty, J.W., Lyons-Cohen, M.R., Jaffe, J.B., DiPeso, L.,
1070 Schneider, C., Miller, C.N., Pollack, J.L., Nagana Gowda, G.A., Fontana, M.F., et al.
1071 (2018). Detection of Succinate by Intestinal Tuft Cells Triggers a Type 2 Innate
1072 Immune Circuit. Immunity *49*, 33-41.e7. 10.1016/j.immuni.2018.06.016.

1073 12. Schütz, B., Ruppert, A.-L., Strobel, O., Lazarus, M., Urade, Y., Büchler, M.W.,
1074 and Weihe, E. (2019). Distribution pattern and molecular signature of cholinergic tuft
1075 cells in human gastro-intestinal and pancreatic-biliary tract. Sci Rep *9*, 17466.
1076 10.1038/s41598-019-53997-3.

1077 13. Deng, J., Tan, L.H., Kohanski, M.A., Kennedy, D.W., Bosso, J.V., Adappa, N.D.,
1078 Palmer, J.N., Shi, J., and Cohen, N.A. (2021). Solitary chemosensory cells are
1079 innervated by trigeminal nerve endings and autoregulated by cholinergic receptors.
1080 Int Forum Allergy Rhinol *11*, 877–884. 10.1002/alr.22695.

1081 14. Tizzano, M., Gulbransen, B.D., Vandenbeuch, A., Clapp, T.R., Herman, J.P.,
1082 Sibhatu, H.M., Churchill, M.E.A., Silver, W.L., Kinnamon, S.C., and Finger, T.E.
1083 (2010). Nasal chemosensory cells use bitter taste signaling to detect irritants and
1084 bacterial signals. Proc Natl Acad Sci U S A *107*, 3210–3215.
1085 10.1073/pnas.0911934107.

1086 15. Saunders, C.J., Christensen, M., Finger, T.E., and Tizzano, M. (2014).
1087 Cholinergic neurotransmission links solitary chemosensory cells to nasal
1088 inflammation. Proc Natl Acad Sci U S A *111*, 6075–6080. 10.1073/pnas.1402251111.

1089 16. Krasteva, G., Canning, B.J., Hartmann, P., Veres, T.Z., Papadakis, T., Mühlfeld,
1090 C., Schliecker, K., Tallini, Y.N., Braun, A., Hackstein, H., et al. (2011). Cholinergic
1091 chemosensory cells in the trachea regulate breathing. Proc Natl Acad Sci U S A *108*,
1092 9478–9483. 10.1073/pnas.1019418108.

1093 17. Hollenhorst, M.I., Jurastow, I., Nandigama, R., Appenzeller, S., Li, L., Vogel, J.,
1094 Wiederhold, S., Althaus, M., Empting, M., Altmüller, J., et al. (2020). Tracheal brush
1095 cells release acetylcholine in response to bitter tastants for paracrine and autocrine
1096 signaling. FASEB J *34*, 316–332. 10.1096/fj.201901314RR.

1097 18. Lips, K.S., Wunsch, J., Zarghooni, S., Bschleipfer, T., Schukowski, K., Weidner,
1098 W., Wessler, I., Schwantes, U., Koepsell, H., and Kummer, W. (2007). Acetylcholine
1099 and molecular components of its synthesis and release machinery in the urothelium.
1100 Eur Urol *51*, 1042–1053. 10.1016/j.eururo.2006.10.028.

1101 19. Deckmann, K., Filipski, K., Krasteva-Christ, G., Fronius, M., Althaus, M., Rafiq,
1102 A., Papadakis, T., Renno, L., Jurastow, I., Wessels, L., et al. (2014). Bitter triggers
1103 acetylcholine release from polymodal urethral chemosensory cells and bladder
1104 reflexes. Proc Natl Acad Sci U S A *111*, 8287–8292. 10.1073/pnas.1402436111.

1105 20. Gerbe, F., Sidot, E., Smyth, D.J., Ohmoto, M., Matsumoto, I., Dardalhon, V.,
1106 Cesses, P., Garnier, L., Pouzolles, M., Brulin, B., et al. (2016). Intestinal epithelial tuft
1107 cells initiate type 2 mucosal immunity to helminth parasites. Nature *529*, 226–230.
1108 10.1038/nature16527.

1109 21. von Moltke, J., Ji, M., Liang, H.-E., and Locksley, R.M. (2016). Tuft-cell-derived
1110 IL-25 regulates an intestinal ILC2-epithelial response circuit. Nature *529*, 221–225.
1111 10.1038/nature16161.

1112 22. Howitt, M.R., Lavoie, S., Michaud, M., Blum, A.M., Tran, S.V., Weinstock, J.V.,
1113 Gallini, C.A., Redding, K., Margolskee, R.F., Osborne, L.C., et al. (2016). Tuft cells,
1114 taste-chemosensory cells, orchestrate parasite type 2 immunity in the gut. Science
1115 *351*, 1329–1333. 10.1126/science.aaf1648.

1116 23. Schneider, C., O'Leary, C.E., von Moltke, J., Liang, H.-E., Ang, Q.Y., Turnbaugh,
1117 P.J., Radhakrishnan, S., Pellizzon, M., Ma, A., and Locksley, R.M. (2018). A
1118 Metabolite-Triggered Tuft Cell-ILC2 Circuit Drives Small Intestinal Remodeling. Cell
1119 *174*, 271-284.e14. 10.1016/j.cell.2018.05.014.

1120 24. Lei, W., Ren, W., Ohmoto, M., Urban, J.F., Matsumoto, I., Margolskee, R.F., and
1121 Jiang, P. (2018). Activation of intestinal tuft cell-expressed Sucnr1 triggers type 2
1122 immunity in the mouse small intestine. Proc Natl Acad Sci U S A *115*, 5552–5557.
1123 10.1073/pnas.1720758115.

1124 25. Hofmann, T., Chubanov, V., Gudermann, T., and Montell, C. (2003). TRPM5 is a
1125 voltage-modulated and Ca(2+)-activated monovalent selective cation channel. Curr
1126 Biol *13*, 1153–1158. 10.1016/s0960-9822(03)00431-7.

1127 26. O'Leary, C.E., Schneider, C., and Locksley, R.M. (2019). Tuft Cells-Systemically
1128 Dispersed Sensory Epithelia Integrating Immune and Neural Circuitry. Annu Rev
1129 Immunol *37*, 47–72. 10.1146/annurev-immunol-042718-041505.

1130 27. McGinty, J.W., Ting, H.-A., Billipp, T.E., Nadjsombati, M.S., Khan, D.M., Barrett,
1131 N.A., Liang, H.-E., Matsumoto, I., and von Moltke, J. (2020). Tuft-Cell-Derived
1132 Leukotrienes Drive Rapid Anti-helminth Immunity in the Small Intestine but Are
1133 Dispensable for Anti-protist Immunity. Immunity *52*, 528-541.e7.
1134 10.1016/j.immuni.2020.02.005.

1135 28. Marillier, R.G., Michels, C., Smith, E.M., Fick, L.C.E., Leeto, M., Dewals, B.,
1136 Horsnell, W.G.C., and Brombacher, F. (2008). IL-4/IL-13 independent goblet cell
1137 hyperplasia in experimental helminth infections. BMC Immunol *9*, 11. 10.1186/1471-
1138 2172-9-11.

1139 29. McKenzie, G.J., Bancroft, A., Grencis, R.K., and McKenzie, A.N. (1998). A
1140 distinct role for interleukin-13 in Th2-cell-mediated immune responses. Curr Biol *8*,
1141 339–342. 10.1016/s0960-9822(98)70134-4.

1142 30. Miller, H.R., Huntley, J.F., and Wallace, G.R. (1981). Immune exclusion and
1143 mucus trapping during the rapid expulsion of Nippostrongylus brasiliensis from
1144 primed rats. Immunology *44*, 419–429.

1145 31. Grencis, R.K. (2015). Immunity to Helminths: Resistance, Regulation, and
1146 Susceptibility to Gastrointestinal Nematodes. Annual Review of Immunology *33*, 201–
1147 225. 10.1146/annurev-immunol-032713-120218.

1148 32. Oeser, K., Schwartz, C., and Voehringer, D. (2015). Conditional IL-4/IL-13-
1149 deficient mice reveal a critical role of innate immune cells for protective immunity

1150 against gastrointestinal helminths. Mucosal Immunol *8*, 672–682.
1151 10.1038/mi.2014.101.

1152 33. Herbert, D.R., Yang, J.-Q., Hogan, S.P., Groschwitz, K., Khodoun, M., Munitz, A.,
1153 Orekov, T., Perkins, C., Wang, Q., Brombacher, F., et al. (2009). Intestinal epithelial
1154 cell secretion of RELM-beta protects against gastrointestinal worm infection. J Exp
1155 Med *206*, 2947–2957. 10.1084/jem.20091268.

1156 34. Hu, Z., Zhang, C., Sifuentes-Dominguez, L., Zarek, C.M., Propheter, D.C.,
1157 Kuang, Z., Wang, Y., Pendse, M., Ruhn, K.A., Hassell, B., et al. (2021). Small
1158 proline-rich protein 2A is a gut bactericidal protein deployed during helminth infection.
1159 Science (New York, N.Y.) *374*, eabe6723. 10.1126/science.abe6723.

1160 35. Wu, D., Ahrens, R., Osterfeld, H., Noah, T.K., Groschwitz, K., Foster, P.S.,
1161 Steinbrecher, K.A., Rothenberg, M.E., Shroyer, N.F., Matthaei, K.I., et al. (2011).
1162 Interleukin-13 (IL-13)/IL-13 receptor alpha1 (IL-13Ralpha1) signaling regulates
1163 intestinal epithelial cystic fibrosis transmembrane conductance regulator channel-
1164 dependent Cl- secretion. J Biol Chem *286*, 13357–13369. 10.1074/jbc.M110.214965.

1165 36. Horsnell, W.G.C., Cutler, A.J., Hoving, J.C., Mearns, H., Myburgh, E., Arendse,
1166 B., Finkelman, F.D., Owens, G.K., Erle, D., and Brombacher, F. (2007). Delayed
1167 goblet cell hyperplasia, acetylcholine receptor expression, and worm expulsion in
1168 SMC-specific IL-4Ralpha-deficient mice. PLoS Pathog *3*, e1.
1169 10.1371/journal.ppat.0030001.

1170 37. Akiho, H., Blennerhassett, P., Deng, Y., and Collins, S.M. (2002). Role of IL-4, IL-
1171 13, and STAT6 in inflammation-induced hypercontractility of murine smooth muscle
1172 cells. Am J Physiol Gastrointest Liver Physiol *282*, G226-232.
1173 10.1152/ajpgi.2002.282.2.G226.

1174 38. Zhao, A., McDermott, J., Urban, J.F., Gause, W., Madden, K.B., Yeung, K.A.,
1175 Morris, S.C., Finkelman, F.D., and Shea-Donohue, T. (2003). Dependence of IL-4, IL-
1176 13, and nematode-induced alterations in murine small intestinal smooth muscle
1177 contractility on Stat6 and enteric nerves. J Immunol *171*, 948–954.
1178 10.4049/jimmunol.171.2.948.

1179 39. Darby, M., Schnoeller, C., Vira, A., Culley, F.J., Bobat, S., Logan, E., Kirstein, F.,
1180 Wess, J., Cunningham, A.F., Brombacher, F., et al. (2015). The M3 muscarinic
1181 receptor is required for optimal adaptive immunity to helminth and bacterial infection.
1182 PLoS Pathog *11*, e1004636. 10.1371/journal.ppat.1004636.

1183 40. McLean, L.P., Smith, A., Cheung, L., Urban, J.F., Sun, R., Grinchuk, V., Desai,
1184 N., Zhao, A., Raufman, J.-P., and Shea-Donohue, T. (2016). Type 3 muscarinic
1185 receptors contribute to intestinal mucosal homeostasis and clearance of
1186 Nippostrongylus brasiliensis through induction of TH2 cytokines. Am J Physiol
1187 Gastrointest Liver Physiol *311*, G130-141. 10.1152/ajpgi.00461.2014.

1188 41. Sanderson, B.E., and Ogilvie, B.M. (1971). A study of acetylcholinesterase
1189 throughout the life cycle of Nippostrongylus brasiliensis. Parasitology *62*, 367–373.
1190 10.1017/s0031182000077519.

1191 42. Blackburn, C.C., and Selkirk, M.E. (1992). Characterisation of the secretory
1192 acetylcholinesterases from adult Nippostrongylus brasiliensis. Mol Biochem Parasitol
1193 *53*, 79–88. 10.1016/0166-6851(92)90009-9.

1194 43. Lawrence, C.E., and Pritchard, D.I. (1993). Differential secretion of
1195 acetylcholinesterase and proteases during the development of Heligmosomoides
1196 polygyrus. Int J Parasitol *23*, 309–314. 10.1016/0020-7519(93)90004-i.

1197 44. Nadjsombati, M.S., Niepoth, N., Webeck, L.M., Kennedy, E.A., Jones, D.L.,
1198 Baldridge, M.T., Bendesky, A., and Moltke, J. von (2022). Genetic mapping reveals
1199 Pou2af2-dependent tuning of tuft cell differentiation and intestinal type 2 immunity.
1200 2022.10.19.512785. 10.1101/2022.10.19.512785.

1201 45. von Moltke, J., Ji, M., Liang, H.-E., and Locksley, R.M. (2016). Tuft-cell-derived
1202 IL-25 regulates an intestinal ILC2-epithelial response circuit. Nature *529*, 221–225.
1203 10.1038/nature16161.

1204 46. Specian, R.D., and Neutra, M.R. (1980). Mechanism of rapid mucus secretion in
1205 goblet cells stimulated by acetylcholine. J Cell Biol *85*, 626–640.
1206 10.1083/jcb.85.3.626.

1207 47. Gustafsson, J.K., Ermund, A., Johansson, M.E.V., Schütte, A., Hansson, G.C.,
1208 and Sjövall, H. (2012). An ex vivo method for studying mucus formation, properties,
1209 and thickness in human colonic biopsies and mouse small and large intestinal
1210 explants. Am J Physiol Gastrointest Liver Physiol *302*, G430-438.
1211 10.1152/ajpgi.00405.2011.

1212 48. Stockinger, S., Albers, T., Duerr, C.U., Ménard, S., Pütsep, K., Andersson, M.,
1213 and Hornef, M.W. (2014). Interleukin-13-mediated paneth cell degranulation and
1214 antimicrobial peptide release. J Innate Immun *6*, 530–541. 10.1159/000357644.

1215 49. Hubel, K.A. (1976). Intestinal ion transport: effect of norepinephrine, pilocarpine,
1216 and atropine. Am J Physiol *231*, 252–257. 10.1152/ajplegacy.1976.231.1.252.

1217 50. Banks, M.R., and Farthing, M.J.G. (2002). Fluid and electrolyte transport in the
1218 small intestine. Curr Opin Gastroenterol *18*, 176–181. 10.1097/00001574-
1219 200203000-00004.

1220 51. Clarke, L.L. (2009). A guide to Ussing chamber studies of mouse intestine. Am J
1221 Physiol Gastrointest Liver Physiol *296*, G1151-1166. 10.1152/ajpgi.90649.2008.

1222 52. Browning, J.G., Hardcastle, J., Hardcastle, P.T., and Redfern, J.S. (1978).
1223 Localization of the effect of acetylcholine in regulating intestinal ion transport. J
1224 Physiol *281*, 15–27. 10.1113/jphysiol.1978.sp012406.

1225 53. Geubelle, P., Gilissen, J., Dilly, S., Poma, L., Dupuis, N., Laschet, C., Abboud,
1226 D., Inoue, A., Jouret, F., Pirotte, B., et al. (2017). Identification and pharmacological
1227 characterization of succinate receptor agonists. Br J Pharmacol *174*, 796–808.
1228 10.1111/bph.13738.

1229 54. Vanoye, C.G., Altenberg, G.A., and Reuss, L. (1999). Inhibition of P-glycoprotein-
1230 mediated transport by a hydrophobic contaminant in commercial gluconate salts. Am
1231 J Physiol *276*, C1439-1442. 10.1152/ajpcell.1999.276.6.C1439.

1232 55. Harrington, A.M., Hutson, J.M., and Southwell, B.R. (2010). Cholinergic
1233 neurotransmission and muscarinic receptors in the enteric nervous system. Prog
1234 Histochem Cytochem *44*, 173–202. 10.1016/j.proghi.2009.10.001.

1235 56. Xiong, Z., Zhu, X., Geng, J., Xu, Y., Wu, R., Li, C., Fan, D., Qin, X., Du, Y., Tian,
1236 Y., et al. (2022). Intestinal Tuft-2 cells exert antimicrobial immunity via sensing
1237 bacterial metabolite N-undecanoylglycine. Immunity *55*, 686-700.e7.
1238 10.1016/j.immuni.2022.03.001.

1239 57. Keshavarz, M., Faraj Tabrizi, S., Ruppert, A.-L., Pfeil, U., Schreiber, Y., Klein, J.,
1240 Brandenburger, I., Lochnit, G., Bhushan, S., Perniss, A., et al. (2022). Cysteinyl
1241 leukotrienes and acetylcholine are biliary tuft cell cotransmitters. Sci Immunol *7*,
1242 eabf6734. 10.1126/sciimmunol.abf6734.

1243 58. Lee, R.J., Kofonow, J.M., Rosen, P.L., Siebert, A.P., Chen, B., Doghramji, L.,
1244 Xiong, G., Adappa, N.D., Palmer, J.N., Kennedy, D.W., et al. (2014). Bitter and sweet
1245 taste receptors regulate human upper respiratory innate immunity. J. Clin. Invest.
1246 *124*, 1393–1405. 10.1172/JCI72094.

1247 59. Zhu, H., Aryal, D.K., Olsen, R.H.J., Urban, D.J., Swearingen, A., Forbes, S.,
1248 Roth, B.L., and Hochgeschwender, U. (2016). Cre-dependent DREADD (Designer
1249 Receptors Exclusively Activated by Designer Drugs) mice. Genesis *54*, 439–446.
1250 10.1002/dvg.22949.

1251 60. Chen, X., Choo, H., Huang, X.-P., Yang, X., Stone, O., Roth, B.L., and Jin, J.
1252 (2015). The first structure-activity relationship studies for designer receptors
1253 exclusively activated by designer drugs. ACS Chem Neurosci *6*, 476–484.
1254 10.1021/cn500325v.

1255 61. Barilli, A., Aldegheri, L., Bianchi, F., Brault, L., Brodbeck, D., Castelletti, L.,
1256 Feriani, A., Lingard, I., Myers, R., Nola, S., et al. (2021). From High-Throughput
1257 Screening to Target Validation: Benzo[d]isothiazoles as Potent and Selective
1258 Agonists of Human Transient Receptor Potential Cation Channel Subfamily M
1259 Member 5 Possessing In Vivo Gastrointestinal Prokinetic Activity in Rodents. J Med
1260 Chem *64*, 5931–5955. 10.1021/acs.jmedchem.1c00065.

1261 62. Virginio, C., Aldegheri, L., Nola, S., Brodbeck, D., Brault, L., Raveglia, L.F.,
1262 Barilli, A., Sabat, M., and Myers, R. (2022). Identification of positive modulators of

1263 TRPM5 channel from a high-throughput screen using a fluorescent membrane
1264 potential assay. SLAS Discov *27*, 55–64. 10.1016/j.slasd.2021.10.004.

1265 63. Wyatt, K.D., Sakamoto, K., and Watford, W.T. (2022). Tamoxifen administration
1266 induces histopathologic changes within the lungs of Cre-recombinase-negative mice:
1267 A case report. Lab Anim *56*, 297–303. 10.1177/00236772211042968.

1268 64. Chu, C., Parkhurst, C.N., Zhang, W., Zhou, L., Yano, H., Arifuzzaman, M., and
1269 Artis, D. (2021). The ChAT-acetylcholine pathway promotes group 2 innate lymphoid
1270 cell responses and anti-helminth immunity. Sci Immunol *6*, eabe3218.
1271 10.1126/sciimmunol.abe3218.

1272 65. Roberts, L.B., Schnoeller, C., Berkachy, R., Darby, M., Pillaye, J., Oudhoff, M.J.,
1273 Parmar, N., Mackowiak, C., Sedda, D., Quesniaux, V., et al. (2021). Acetylcholine
1274 production by group 2 innate lymphoid cells promotes mucosal immunity to
1275 helminths. Sci Immunol *6*, eabd0359. 10.1126/sciimmunol.abd0359.

1276 66. C, S., Dj, T., and Rk, G. (2018). A sticky end for gastrointestinal helminths; the
1277 role of the mucus barrier. Parasite immunology *40*. 10.1111/pim.12517.

1278 67. Middelhoff, M., Nienhüser, H., Valenti, G., Maurer, H.C., Hayakawa, Y.,
1279 Takahashi, R., Kim, W., Jiang, Z., Malagola, E., Cuti, K., et al. (2020). Prox1-positive
1280 cells monitor and sustain the murine intestinal epithelial cholinergic niche. Nat
1281 Commun *11*, 111. 10.1038/s41467-019-13850-7.

1282 68. Takahashi, T., Shiraishi, A., Murata, J., Matsubara, S., Nakaoka, S., Kirimoto, S.,
1283 and Osawa, M. (2021). Muscarinic receptor M3 contributes to intestinal stem cell
1284 maintenance via EphB/ephrin-B signaling. Life Sci Alliance *4*, e202000962.
1285 10.26508/lsa.202000962.

1286 69. Madden, K.B., Yeung, K.A., Zhao, A., Gause, W.C., Finkelman, F.D., Katona,
1287 I.M., Urban, J.F., and Shea-Donohue, T. (2004). Enteric nematodes induce
1288 stereotypic STAT6-dependent alterations in intestinal epithelial cell function. J
1289 Immunol *172*, 5616–5621. 10.4049/jimmunol.172.9.5616.

1290 70. Schütz, B., Jurastow, I., Bader, S., Ringer, C., von Engelhardt, J., Chubanov, V.,
1291 Gudermann, T., Diener, M., Kummer, W., Krasteva-Christ, G., et al. (2015). Chemical
1292 coding and chemosensory properties of cholinergic brush cells in the mouse
1293 gastrointestinal and biliary tract. Front Physiol *6*, 87. 10.3389/fphys.2015.00087.

1294 71. Jk, G., A, E., D, A., Me, J., He, N., K, T., H, H., H, S., and Gc, H. (2012).
1295 Bicarbonate and functional CFTR channel are required for proper mucin secretion
1296 and link cystic fibrosis with its mucus phenotype. The Journal of experimental
1297 medicine *209*. 10.1084/jem.20120562.

1298 72. Birchenough, G.M.H., Johansson, M.E.V., Gustafsson, J.K., Bergström, J.H., and
1299 Hansson, G.C. (2015). New developments in goblet cell mucus secretion and
1300 function. Mucosal Immunol *8*, 712–719. 10.1038/mi.2015.32.

1301 73. Knoop, K.A., McDonald, K.G., McCrate, S., McDole, J.R., and Newberry, R.D.
1302 (2015). Microbial sensing by goblet cells controls immune surveillance of luminal
1303 antigens in the colon. Mucosal Immunol *8*, 198–210. 10.1038/mi.2014.58.

1304 74. Gustafsson, J.K., Davis, J.E., Rappai, T., McDonald, K.G., Kulkarni, D.H., Knoop,
1305 K.A., Hogan, S.P., Fitzpatrick, J.A., Lencer, W.I., and Newberry, R.D. (2021).
1306 Intestinal goblet cells sample and deliver lumenal antigens by regulated endocytic
1307 uptake and transcytosis. Elife *10*, e67292. 10.7554/eLife.67292.

1308 75. Dolan, B., Ermund, A., Martinez-Abad, B., Johansson, M.E.V., and Hansson,
1309 G.C. (2022). Clearance of small intestinal crypts involves goblet cell mucus secretion
1310 by intracellular granule rupture and enterocyte ion transport. Sci Signal *15*, eabl5848.
1311 10.1126/scisignal.abl5848.

1312 76. Birchenough, G.M.H., Nyström, E.E.L., Johansson, M.E.V., and Hansson, G.C.
1313 (2016). A sentinel goblet cell guards the colonic crypt by triggering Nlrp6-dependent
1314 Muc2 secretion. Science *352*, 1535–1542. 10.1126/science.aaf7419.

1315 77. Morroni, M., Cangiotti, A.M., and Cinti, S. (2007). Brush cells in the human
1316 duodenojejunal junction: an ultrastructural study. J Anat *211*, 125–131.
1317 10.1111/j.1469-7580.2007.00738.x.

1318 78. Cheng, X., Voss, U., and Ekblad, E. (2018). Tuft cells: Distribution and
1319 connections with nerves and endocrine cells in mouse intestine. Exp Cell Res *369*,
1320 105–111. 10.1016/j.yexcr.2018.05.011.

1321 79. Hollenhorst, M.I., Kumar, P., Zimmer, M., Salah, A., Maxeiner, S., Elhawy, M.I.,
1322 Evers, S.B., Flockerzi, V., Gudermann, T., Chubanov, V., et al. (2022). Taste
1323 Receptor Activation in Tracheal Brush Cells by Denatonium Modulates ENaC
1324 Channels via Ca2+, cAMP and ACh. Cells *11*, 2411. 10.3390/cells11152411.

1325 80. Banerjee, A., Herring, C.A., Chen, B., Kim, H., Simmons, A.J., Southard-Smith,
1326 A.N., Allaman, M.M., White, J.R., Macedonia, M.C., Mckinley, E.T., et al. (2020).
1327 Succinate Produced by Intestinal Microbes Promotes Specification of Tuft Cells to
1328 Suppress Ileal Inflammation. Gastroenterology *159*, 2101-2115.e5.
1329 10.1053/j.gastro.2020.08.029.

1330 81. Huh, W.J., Roland, J.T., Asai, M., and Kaji, I. (2020). Distribution of duodenal tuft
1331 cells is altered in pediatric patients with acute and chronic enteropathy. Biomedical
1332 Research *41*, 113–118. 10.2220/biomedres.41.113.

1333 82. Aigbologa, J., Connolly, M., Buckley, J.M., and O'Malley, D. (2020). Mucosal Tuft
1334 Cell Density Is Increased in Diarrhea-Predominant Irritable Bowel Syndrome Colonic
1335 Biopsies. Front Psychiatry *11*, 436. 10.3389/fpsyt.2020.00436.

1336 83. Fung, C., Fraser, L.M., Barrón, G.M., Gologorsky, M.B., Atkinson, S.N., Gerrick,
1337 E.R., Hayward, M., Ziegelbauer, J., Li, J.A., Nico, K.F., et al. (2022). Tuft cells

1338 mediate commensal remodeling of the small intestinal antimicrobial landscape.
1339 2022.10.24.512770. 10.1101/2022.10.24.512770.

1340 84. Sa, R., C, L., Am, M., K, L., Kl, T., C, B., S, K., Sk, G., A, N., Jm, A.-G., et al.
1341 (2019). CFTR-PTEN-dependent mitochondrial metabolic dysfunction promotes
1342 Pseudomonas aeruginosa airway infection. Science translational medicine *11*.
1343 10.1126/scitranslmed.aav4634.

1344 85. Voehringer, D., Reese, T.A., Huang, X., Shinkai, K., and Locksley, R.M. (2006).
1345 Type 2 immunity is controlled by IL-4/IL-13 expression in hematopoietic non-
1346 eosinophil cells of the innate immune system. J Exp Med *203*, 1435–1446.
1347 10.1084/jem.20052448.

1348 86. Me, K., Cm, M., Jg, G., Sd, P., An, G., R, A., S, Y., Pe, B., Ca, S., Pl, Z., et al.
1349 (2022). IL-13-programmed airway tuft cells produce PGE2, which promotes CFTR-
1350 dependent mucociliary function. JCI insight *7*. 10.1172/jci.insight.159832.

1351 87. Nadjsombati, M.S., McGinty, J.W., Lyons-Cohen, M.R., Jaffe, J.B., DiPeso, L.,
1352 Schneider, C., Miller, C.N., Pollack, J.L., Nagana Gowda, G.A., Fontana, M.F., et al.
1353 (2018). Detection of Succinate by Intestinal Tuft Cells Triggers a Type 2 Innate
1354 Immune Circuit. Immunity *49*, 33-41.e7. 10.1016/j.immuni.2018.06.016.

1355 88. Chudnovskiy, A., Mortha, A., Kana, V., Kennard, A., Ramirez, J.D., Rahman, A.,
1356 Remark, R., Mogno, I., Ng, R., Gnjatic, S., et al. (2016). Host-Protozoan Interactions
1357 Protect from Mucosal Infections through Activation of the Inflammasome. Cell *167*,
1358 444-456.e14. 10.1016/j.cell.2016.08.076.

1359 89. Law, C.W., Chen, Y., Shi, W., and Smyth, G.K. (2014). voom: Precision weights
1360 unlock linear model analysis tools for RNA-seq read counts. Genome Biol *15*, R29.
1361 10.1186/gb-2014-15-2-r29.

1362 90. Robinson, M.D., and Oshlack, A. (2010). A scaling normalization method for
1363 differential expression analysis of RNA-seq data. Genome Biol *11*, R25. 10.1186/gb-
1364 2010-11-3-r25.

1365 91. Robinson, M.D., McCarthy, D.J., and Smyth, G.K. (2010). edgeR: a Bioconductor
1366 package for differential expression analysis of digital gene expression data.
1367 Bioinformatics *26*, 139–140. 10.1093/bioinformatics/btp616.

1368 92. Ritchie, M.E., Phipson, B., Wu, D., Hu, Y., Law, C.W., Shi, W., and Smyth, G.K.
1369 (2015). limma powers differential expression analyses for RNA-sequencing and
1370 microarray studies. Nucleic Acids Res *43*, e47. 10.1093/nar/gkv007.

1371